American Journal of Science

MODELING THE CONSEQUENCES OF LAND PLANT EVOLUTION ON SILICATE WEATHERING

DANIEL E. IBARRA*,**,‡,†, JEREMY K. CAVES RUGENSTEIN*,***,#,‡,†,
AVIV BACHAN**,‡,†, ANDRÉS BARESCH**, KIMBERLY V. LAU**,§,##,
DANA L. THOMAS**,§§, JUNG-EUN LEE§§§, C. KEVIN BOYCE**,
and C. PAGE CHAMBERLAIN*,**

ABSTRACT. It has long been recognized that the advent of vascular plants in the Paleozoic must have changed silicate weathering and fundamentally altered the long-term carbon cycle. Carbon cycle models are frequently employed to quantify the effect of this state change in the Earth system. These models have suggested that plants likely played a key role in modulating atmospheric CO_2 in the past, with the largest plant-induced changes to the system in the late Paleozoic. These studies have, for the most part, focused on the effects of plants on weathering via their impacts on the soil environment. Yet, plants also modify the hydrological cycle, which may also have had implications for global weathering. Here, we evaluate the consequences of plant evolutionary innovation that have not been previously incorporated into carbon cycle models by coupling a one-dimensional vapor transport model to a reactive transport model of silicate weathering. Using this cascade of models, we investigate: 1) how evolutionary shifts in plant transpiration may have enhanced silicate weathering through increased downwind transport of water vapor to continental interiors; 2) the importance of deeply-rooted plants and their associated microbial communities in increasing soil CO_2 and weathering zone length scales; and, 3) the coupled effect of these two processes on weathering rates.

The hydrologic balance for our modeling approach is framed by energy/supply constraints (encapsulated through Budyko relationships) calibrated for minimally vegetated-, vascular plant forested-, and angiosperm-worlds. Using constraints for atmospheric vapor-transport over continents and terrestrial weathering fluxes, we find that the emergence of widespread transpiration and associated inland vapor recycling associated with the advent of deep-rooted vascular plants over the later Devonian increases weathering solute concentrations by a factor of 1.64 to 2.39 for a fixed atmospheric CO_2. The later domination of ecosystems by angiosperms in the late Cretaceous and Cenozoic, and the subsequent increase in transpiration fluxes, increased weathering solute concentrations by 7 to 55 percent leading to a cumulative total increase in weathering solute concentrations by a factor of 1.70 to 2.55. Partitioning of the vapor recycling effects and feedbacks on the weathering thermodynamics

* Department of Earth System Science, Stanford University, Stanford, California 94305, USA
** Department of Geological Sciences, Stanford University, Stanford, California 94305, USA
*** Department of Earth Sciences, Swiss Federal Institute of Technology (ETH) Zürich, 8092 Zürich, Switzerland
§ Department of Earth Sciences, University of California Riverside, Riverside, California 92521, USA
§§ Jackson School of Geosciences, University of Texas at Austin, Austin, Texas 78712, USA
§§§ Department of Earth, Environmental and Planetary Sciences, Brown University, Rhode Island 02912, USA
# Present address: Max Planck Institute for Meteorology, Bundesstrasse 53, 20146 Hamburg, Germany
Present address: Department of Geology and Geophysics, University of Wyoming, Laramie, Wyoming 82071
† Corresponding authors: danieli@stanford.edu; jeremy.caves@gmail.com; aviv.bachan@gmail.com
‡ These authors contributed equally to this work.

indicates that 55 percent of the increases in weathering concentrations are due to the thermodynamic effects of soil CO_2 with the remaining 45 percent attributable to hydrologic effects. Our estimates of the relative changes in weathering solute concentrations caused by land plant evolution are of a similar magnitude to relative flux scaling relationships implemented in existing carbon cycle models such as GEOCARBSULF (Berner, 2006), COPSE (Bergman and others, 2004), and GEOCLIM (Le Hir and others, 2011). As Phanerozoic plant evolution resulted in a more efficient generation of weathering solutes, a weaker dependence of silicate weathering on physical forcing factors such as temperature, pH of rainwater, tectonics, and prevailing lithology, must have resulted. Consequently, we postulate that terrestrial plant evolution likely contributed to a more stable climate system over the Phanerozoic.

INTRODUCTION

Earth's climate has been remarkably stable over the last 4 billion year history. The relative stability of the Earth's climate has been attributed to a negative feedback on climate imposed by the weathering of silicate rocks (for example, Walker and others, 1981; Berner and others, 1983; Berner 1991, 2004, 2006; Berner and Caldeira, 1997; Maher and Chamberlain, 2014). Weathering reactions occur subaerially, and to a lesser degree in association with hydrothermal systems in the ocean (Coogan and Gillis, 2013; Mills and others, 2014). Weathering reactions convert carbon in the ocean-atmosphere system to carbonate alkalinity (bicarbonate, HCO_3^-, and carbonate, CO_3^{2-}, ions), which then combine with cations (primarily Ca^{2+} and Mg^{2+}) that are deposited as calcium and magnesium carbonate in marine sediments. The net result is the removal of carbon from the ocean-atmosphere to the solid Earth (Urey, 1952; Zeebe and Caldeira, 2008)—a process that is often referred to as the silicate weathering negative feedback where increased CO_2 concentrations lead to more efficient removal of CO_2 via silicate weathering. The overall weatherability of the Earth surface determines the efficiency with which silicate weathering converts CO_2 to bicarbonate through reaction with subaerially exposed silicate rocks. This weatherability is determined by two primary factors: *(1)* the reactivity of rocks within the weathering zone and *(2)* the areal extent and distribution of continents subject to weathering processes. All else being equal, greater reactivity of rocks and larger continental area will result in enhanced weatherability, which results in a lower steady-state $p$$CO_2$. Moreover, the stronger negative feedback, the coupling between silicate weathering fluxes and climate, should provide greater resistance to CO_2 perturbations (Kump and Arthur, 1997; Caves and others, 2016a).

Yet, physical determinants of weatherability such as continental emergence, tectonics, and variations in the lithologic character of exposed rocks, are cyclical processes over geologic time lacking unidirectional state changes (Kump and Arthur, 1997; Gibbs and others, 1999; Kump and others, 2000; Berner, 2006, 2008; Mills and others, 2014; Ibarra and others, 2016; Lee and others, 2018). In contrast, there is unambiguous evidence for biological influences on the weathering zone, including the physical and chemical influence of land plants, which have dramatically and unidirectionally changed through geologic time (Berner, 1987; Schwartzman and Volk, 1989; Volk, 1989; Berner, 1992; Algeo and others, 1995; Algeo and Scheckler, 1998; Knoll, 2003; Pagani and others, 2009; Le Hir and others, 2011; Taylor and others, 2012; Boyce and Lee, 2017).

Land plants are thought to alter weatherability through two key mechanisms (Berner, 1987, 1992; Drever, 1994). First, plants and associated soil microbes enhance weathering directly (Barker and others, 1997). This biota respires CO_2, resulting in $p$$CO_2$ levels in soils that are often several orders of magnitude greater than atmospheric $p$$CO_2$ (Brook and others, 1983; Kelly and others, 1998; Montañez, 2013) and

providing a critical source of protons that contribute to the weathering of rocks (Moulton and Berner, 1998; Moulton and others, 2000; Andrews and Schlesinger, 2001; Berner and others, 2003). Breakdown of rocks is also enhanced by attack of mineral grains by plant fungal symbionts (Blum and others, 2002; Quirk and others, 2014), which increases the mineral surface area accessible for chemical weathering processes. Second, plants may enhance weathering indirectly by altering global hydrology through transpiration due to the evolution of stomata, vasculature, and deep roots that can access groundwater that would otherwise be shielded from evaporation (Shukla and Mintz, 1982; Lee and Boyce, 2010; Boyce and Lee, 2010, 2017). Transpiration increases precipitation globally (Shukla and Mintz, 1982; Kleidon and others, 2000; Lee and Boyce, 2010; Boyce and Lee, 2010, 2017; Alkama and others 2012), permitting both the transport of water vapor into continental interiors and extensive local recycling of water vapor. Because silicate weathering fluxes are fundamentally mediated by the hydrologic cycle (Bluth and Kump, 1994; White and Blum, 1995; Dessert and others, 2003; Donnadieu and others, 2004; Labat and others, 2004; Le Hir and others, 2011; Maher, 2011; Maher and Chamberlain, 2014; Ibarra and others, 2016), we hypothesize that increases in transpiration may have increased the continental area that is accessed for silicate weathering. In short, not only do plants alter the local weathering environment, but they may also expand the area over which silicate weathering can occur through downstream hydrologic feedbacks and teleconnections (for example, Boyce and Lee, 2010, 2011; Green and others, 2017).

Previous studies have attempted to quantify this role of plants on the silicate weathering feedback in a number of ways. The general approach of early studies was to use empirically (for example, Knoll and James, 1987; Moulton and Berner, 1998) or experimentally (for example, Blum and Lasaga, 1988) derived weathering rates to adjust flux scaling terms in 1-D carbon cycle models for the colonization of continents by vascular plant trees in the Devonian and Carboniferous (Schwartzman and Volk, 1989; Berner 1991, 1992, 2006) and the evolution and expansion of angiosperms in the Cretaceous and Early Tertiary (Volk, 1989). More recent work has utilized global climate models configured with paleo-boundary conditions to examine holistically the effect of land plant evolution and colonization on planetary albedo and hydrology (for example Le Hir and others, 2011). Our approach is distinct from these studies as we explicitly examine the effect of plants on silicate weathering through changing hydrology and compare this to the effect due to changing reaction rates. As first hypothesized by Berner (1992) and Drever (1994), based on early climate modeling results by Shukla and Mintz (1982), colonization of continents by plants must have increased rainfall in the interior of continents through the downstream recycling of water vapor by transpiration and thus have increased global weathering fluxes. For example, plants in a coastal region will locally alter the weathering environment through increased weathering rates. Additionally, their transpiration will increase precipitation in continental interiors. This downwind recycling of water will both supply water to the weathering zone and increase plant productivity, thus increasing soil $p\text{CO}_2$ across wide swaths of continents. Consequently, the presence of land plants may increase the quantity of water in continental interiors available for weathering and increase primary productivity, further contributing to an increase in global weatherability.

To test this hypothesis, we examine the relative contributions of these two mechanisms to silicate weathering using a one-dimensional vapor transport model (Hendricks and others, 2000; Mix and others, 2013; Chamberlain and others, 2014; Winnick and others, 2014) that is linked to a reactive transport model of silicate weathering (Maher, 2011; Maher and Chamberlain, 2014; Ibarra and others, 2016, 2017; Wymore and others, 2017).

In this paper, we are explicitly interested in modeling steady-state solute concentrations from silicate weathering on a continent before and after two major plant evolutionary innovations. Following Berner (1992), we assume a baseline condition (referred to as a minimally vegetated world) of precursor microbial communities that likely colonized continents before the advent of vascular plants in the Silurian (DesMarais, 1990). Specifically, this refers to a land surface with no transpiration or biotic amplification of soil CO_2, but with a vegetated albedo similar to modern. First, we test how weathering changed after the proliferation of deeply rooted (greater than a few centimeters) vascular land plants (particularly gymnosperm seed plants and their likely progymnosperm ancestors) that occurred in the later Devonian and Carboniferous. These non-angiosperm vascular land plants would have allowed for increased total evapotranspiration rates and vapor recycling through the evolution of deep roots to access groundwater and vasculature to transport that water to the stomata to support photosynthetic gas exchange. Second, we examine how the spread and dominance of angiosperms in the Late Cretaceous and Cenozoic (Crane and Lidgard, 1989; Burnham and Johnson, 2004; Jaramillo and others, 2006) affected weathering. We do not attempt to model an un-vegetated 'desert world' scenario (for example, Fraedrich and others, 1999; Kleidon and others, 2000). The large changes in albedo involved in such a scenario generate large changes in temperature and potential evapotranspiration that would obscure our assessment of the importance of plant transpiration (for example, Kleidon and others, 2000; Le Hir and others, 2011; Boyce and Lee, 2017). Thus, we do not consider changes in albedo in our modeling and do not simulate 'desert world' or 'bare world' scenarios.

We focus on how plant evolution affects the concentration of weathering solutes, rather than addressing how plant evolution changes weathering fluxes, to isolate the effect of plants on weatherability (independent of changes in runoff). The weathering flux is related to the concentration of weathering solutes:

$$F_{sil} = q \times C \qquad (1)$$

where F_{sil} is the weathering flux [moles/t], q is runoff [L/t], and C is the concentration of weathered solutes [moles/L]. On geologic timescales (> 1 Ma), F_{sil} must equal the volcanic and metamorphic flux of carbon (Berner and Caldeira, 1997; Broecker and Sanyal, 1998; Zeebe and Caldeira, 2008; Caves and others, 2016a). Runoff, in turn, is controlled by climate, including both the strength of the greenhouse effect and solar insolation, though we note that the colonization of continents by plants will change the radiative balance of the Earth through albedo changes (Fraedrich and others, 1999; Kleidon and others, 2000; Alkama and others, 2012), a factor that we do not consider in this study.

For each of the scenarios, we calculate the change in the concentration of weathered solutes through two linked models (fig. 1): The first model (Model 1) allows (evapo-) transpiration to be treated as a variable with integrated precipitation and vapor recycling parameters as outputs. Specifically, Model 1 consists of an advection-diffusion-reaction atmospheric vapor transport model (Hendricks and others, 2000; Winnick and others, 2014; Chamberlain and others, 2014; see Appendix 1 for derivation and details) with a mass-balance scheme to partition surface water derived from precipitation into runoff and evapotranspiration. The second model (Model 2) resolves the weathering concentrations based on changes to plant/bedrock interaction. Model 2 is based on a recently developed reactive transport-weathering model (see Maher, 2011; Maher and Chamberlain, 2014; Ibarra and others, 2016; Wymore and others, 2017 for details). The coupling of Model 1 and 2 is through a runoff term (q, fig. 1), common to both models (output of Model 1, input into Model 2). Model
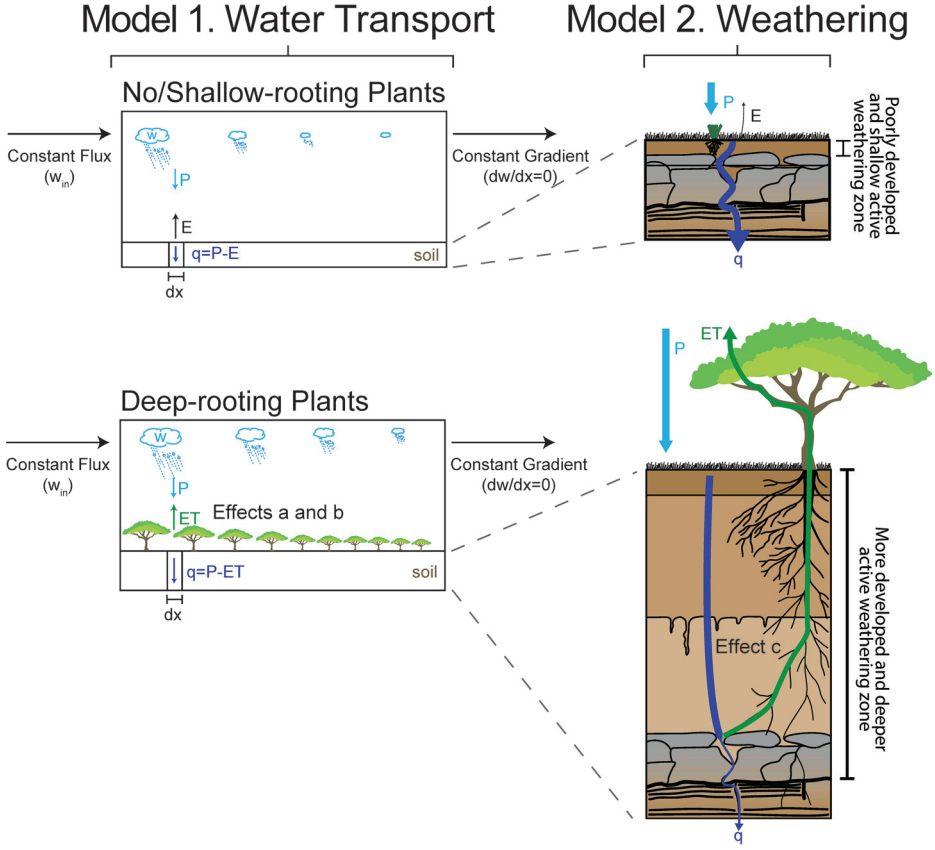
Fig. 1. Schematic of physical set-up of modeling approach for the primary set of boundary conditions (constant flux to constant gradient) considered for Model 1 and the framework for weathering used in Model 2 (see text for details). ET in the lower panels refers to evapotranspiration (ET = E+T, evaporation plus transpiration). Note that throughout the text we denote evaporation (with or without plants) as ET for simplicity.

variables are described in table 1 with assumed values given in table 2. (The Code is available at http://earth.geology.yale.edu/%7eajs/SupplementaryData/2019/Ibarra Code.)

Model 1: Vapor Transport Model

To capture the effect of plants on vapor recycling and downwind precipitation, evapotranspiration, and runoff, we use an advection-diffusion-reaction scheme coupled to a mass-balance formulation of evapotranspiration (*ET*) (*sensu* Budyko) to ensure mass conservation of water (fig. 1, left panels). Following Hendricks and others (2000), we track water vapor in the atmosphere with the following advection-diffusion-reaction equation:

$$\frac{dw}{dt} = \nabla[D\nabla w] - u\nabla w + ET - P \qquad (2)$$

We solve this in steady state, such that $dw/dt = 0$. Here, ∇ is the gradient operator, w [kg/m^2] is the integrated column water vapor, D [m^2/s] is the diffusion coefficient

TABLE 1

Definition and units of model variables

Variable	Description	Units
	Vapor Transport (Model 1)	
w	Column integrated water vapor	kg/m^2
w$_{in}$	Initial (coastal) column water vapor flux	kg/m^2/s
x	Distance from coast	m
T	Transpiration	m/yr
E	Evaporation	m/yr
ω	Adjustable Budyko Parameter	
ET	Evapotranspiration (ET = Evaporation + Transpiration; f(P, E$_p$, ω); equation 4)	m/yr
E$_p$	Potential Evapotranspiration	m/yr
P	Precipitation (P = w*k$_p$)	m/yr
k$_p$	Precipitation rate efficiency	1/s
Q	Discharge	m^3/yr
A	Catchment area	m^2
Pe	Peclet Number (advection to diffusion ratio)	
q	Runoff (specific discharge, q = Q/A)	m/yr
f	Recycling factor (q/P)	
	Weathering Flux (Model 2)	
C$_{max}$	Thermodynamic Maximum Concentration	μmol/L
Dw	Damköhler Coefficient	m/yr
q	Runoff (fed from above Vapor Transport Module)	m/yr

for atmospheric moisture, representing transport by atmospheric eddies, u [m/s] is the velocity, representing the average motion of the atmosphere, P [kg/m^2/s] is precipitation, and ET [kg/m^2/s] is evaporation plus transpiration. We simplify equation 2 by assuming transport along a one-dimensional storm track (left to right in fig. 1, left panel). We further simplify equation 2 by assuming that precipitation (P) is a function of the available water vapor (w), such that:

$$P = k_p \times w \tag{3}$$

where k_p [1/sec] is a precipitation efficiency term scaled to the global average residence time of modern atmospheric vapor ($\sim$ 4.5 days) (Läderach and Sodemann, 2016).

To partition precipitation into ET and q and conserve water mass, we use the Budyko equation (Budyko, 1974; Choudhury, 1999; Zhang and others, 2004; Koster and others, 2006; Gerrits and others, 2009; Greve and others, 2015). This framework allows us to place quantitative bounds on ET and P and is based on water and energy balance equations (Budyko, 1974; Arora, 2002). The form of the one-parameter Budyko equation we use (Choudhury, 1999; Zhang and others, 2004; Greve and others, 2015) is:

$$\frac{ET}{P} = 1 + \frac{E_p}{P} - \left(1 + \left(\frac{E_p}{P} \right)^\omega \right)^{\frac{1}{\omega}} \tag{4}$$

Here, E_p [kg/m^2/s] is potential evapotranspiration and ω is a dimensionless variable ranging from 1 to >5 that characterizes the efficiency with which P is converted to ET. Increasing ω represents increasing efficiency of converting P to ET (Zhang and others, 2004; Koster and others, 2006; Gerrits and others, 2009; Greves and others, 2015).

TABLE 2

Variable constraints for input parameters

Variable	Values Used	Units	Reference
	Water Fluxes (Model 1)		
w_{in}	87.5	kg/m^2/s	Based on control simulations from Boyce and Lee (2010)
ω	1.0 to 3.5+ Pre-Vascular Plants = 1.5 Vascular plant = 2.2 Angiosperm = 2.5		Based on Boyce and Lee (2010) simulations and observations (fig. 2). Modern average of 2.6 also from Greve and others (2015)
E_p	1.0 3.17×10^{-5}	m/yr kg/m^2/s	Based on control simulations from Boyce and Lee (2010)
Pe	1.0		Winnick and others (2014)
k_p	4×10^{-6}	1/s	See below note.
Note: w_{in} and k_p were estimated from atmospheric fluxes in Boyce and Lee (2010, 2017) simulations and assuming a 4.5 day atmospheric moisture residence time (Läderach and Sodemann, 2016).			
	Weathering (Model 2)		
C_{max}	~200 to 1200+	μmol/L	See text, based on relationship with soil pCO$_2$ (fig. A4), Moulton and Berner (1998) (fig. 4), and reactive geochemist workbench simulations (fig. 3)
Dw	Typically 0.003 to 0.5 Modern Cratons = 0.01 Global Average = 0.03 Mountain Maximum = 0.3)	m/yr	Maher and Chamberlain (2014)

Thus, a geologically implausible end-member with no evapotranspiration would be represented by $\omega = 1$ and $ET = 0$, where all water is partitioned to runoff. In contrast, the estimate of ω for the modern world is 2.6 and represents the modern average end member (Greve and others, 2015). To mimic the evolution of plants, we increase ω to capture the effect of increasing transpirative capacity from a minimally-vegetated world (fig. 1, upper panels) to a vascular plant-world to a flora dominated by angiosperms (both fig. 1, lower panels).

Boundary Conditions for Model 1

We apply our hydrologic model over a domain of 10,000 km in length, as this is similar to the zonal length of the large continental landmasses in the late Paleozoic (Domeier and Torsvik, 2014). Our parameterization of the diffusional constant (D) encapsulates a number of complicated processes that are not explicitly resolved in our one-dimensional advection-diffusion-reaction equation and is, further, dependent upon the precise length-scale of interest. Here we calculate D based on modern water isotope observations (Winnick and others, 2014) which suggest that, over mid-latitude areas of continents, both advection and diffusion are roughly equally important in equation 1, corresponding to a Peclet number (Pe = u/D) of 1. Note that the use of 'diffusion' here is more traditionally referred to as 'dispersion' in hydrologic reactive transport modeling, although the use of 'diffusion' to describe this process is consistent with literature on transport of water vapor by atmospheric eddies (for example, Hendricks and others, 2000; Winnick and others, 2014).

To solve the advection-diffusion-reaction equation, we evaluated a series of boundary conditions (see Appendix 1) and present the most realistic set in the main text. We set the boundary condition of a constant water flux (constant flux boundary condition: w_{in} = constant) entering the continent on the western (left) coastal boundary, and for the second boundary condition, we impose no gradient in water vapor exiting the continent on the eastern (right) coastal boundary (no gradient boundary condition: dw/dx = 0). This simulates a situation where the water vapor content has reached equilibrium with respect to transpiration and precipitation and no further net reduction occurs. Some of the precipitated water is returned to the atmosphere via ET and is advected off the continent; consequently, total runoff decreases with increased transpiration as more water vapor is 'lost' at the eastern edge of the continent by advection. Such a decrease in globally-averaged runoff with increasing transpiration is also observed in climate models that evaluate the hydrologic impact of plant evolution (Kleidon and others, 2000; Alkama and others, 2012). In the Appendix, we also show simulations that do not cause total runoff to decrease by imposing constant flux boundary conditions on both edges of the domain, where the western (left) coastal boundary is a positive constant water flux and the eastern (right) boundary is a negative constant water flux leaving the domain.

Because P is a function of w, ET is therefore also a function of w; consequently, there is no analytical solution to the combined set of equations above (equations 2–4). Therefore, we use a numerical discretization scheme to solve the full advection-diffusion-reaction equation (Appendix 1). Values for the above equations are given in table 2 and are derived from the mean terrestrial values from well-constrained climate models and observations (Boyce and Lee 2010, 2017; Greve and others, 2015). We calculate runoff (q) as the difference between P and ET at each grid cell to calculate weathering rates per grid cell (Model 2).

Model 2: Chemical Weathering in Soils

To calculate weathering solute concentrations (C [μmol/L]), we use the solute production equation derived in Maher (2011) and Maher and Chamberlain (2014) (see also Ibarra and others, 2016, 2017; Wymore and others, 2017):

$$C = C_{max} \frac{\tau Dw/q}{1 + \tau Dw/q} \qquad (5)$$

where C_{max} [μmol/L] is the maximum solute concentration for a given aqueous species (for example, SiO_2, HCO_3^-) dictated by the "thermodynamic limit" of the reaction between primary and secondary minerals, q is runoff [m/yr] from Model 1, Dw [m/yr] is the Damköhler coefficient, and τ is an exponential scaling factor derived from an assumption of the water transit time distribution ($\tau = e^2$) (see derivation in Maher and Chamberlain, 2014). The Damköhler coefficient is a measure of the reactivity of the weathering zone and is derived by factoring out runoff from the Damköhler number, which is the ratio of the fluid travel time to the time required to reach equilibrium (see further explanation in Johnson and DePaolo, 1994; Maher and Chamberlain, 2014; Li and others, 2014; Ibarra and others, 2016; Wymore and others, 2017). The Damköhler coefficient [m/yr] is given by:

$$Dw = \frac{L\phi}{T_{eq}} = \frac{R_n L\phi}{C_{max}} \qquad (6)$$

where L is the reactive flowpath length [m], ϕ is the porosity, and T_{eq} is the equilibrium time [years] of the net weathering reaction, which can be related to C_{max} as $T_{eq} = C_{max}/R_n$, where R_n[μmol/L/years] is the net dissolution rate of the weathering

reaction of interest (Maher, 2010, 2011; Maher and Chamberlain, 2014; Ibarra and others, 2016; Wymore and others, 2017). The reactive flowpath length and porosity describe the length of the weathering zone (soil depth in fig. 1).

Using runoff (q) from Model 1, the weathering solute concentration C (eq. 5) is then calculated for each grid cell over our continental landmass. The methods by which C_{max} is calculated are described in the section "Effect c" below. Within this framework, we aim to model the consequences of plants through *(a)* an expansion of water transport across a continent, *(b)* greater local recycling of water vapor, and *(c)* a higher [thermodynamic potential] for chemical weathering. Effects (*a*) and (*b*) capture the effects of plants on hydrology, whereas effect (*c*) focuses on the effects of plants on weathering reactions. Below, we describe how we alter model variables to simulate silicate weathering for our three plant worlds (minimally vegetated world, deeply-rooted vascular plant world, and angiosperm world).

Effect a: Continent-scale Changes in Hydrology (ω) Through Plant Transpiration

In Model 1, we vary ω to capture the effects of increased areal extent of precipitation as transpired water advects inland over 1) a low evaporation, minimally vegetated land surface, 2) a vascular plant world with intermediate evapotranspiration, and 3) an angiosperm world with maximum transpiration capacity (Boyce and Lee, 2010, 2017; fig. 1).
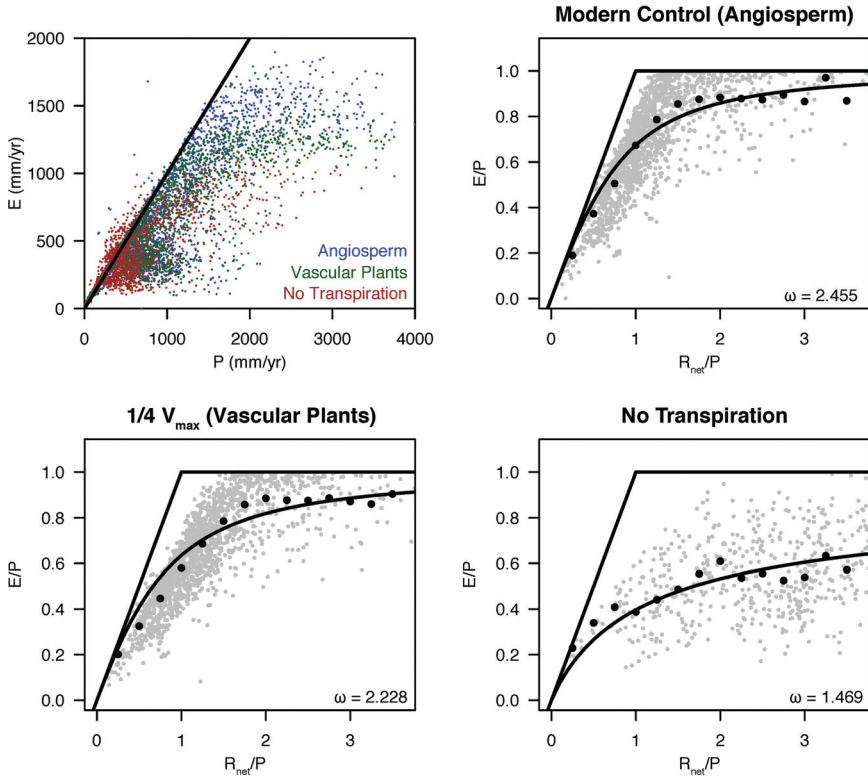
To constrain ω for minimally vegetated-, vascular plant-, and angiosperm-worlds, we use output from climate model simulations that examined the effect of vascular plants and angiosperms on the global hydrological cycle (Boyce and Lee, 2010, 2011; Lee and others, 2012; Boyce and Lee, 2017). As shown in figure 2A, there appears to be a functional limit on *ET* for vascular plants compared to the angiosperm world. We fit equation 4 by solving for the dimensionless quantity (ω) that dictates the form of the equation for different hydrologic environments (figs. 2A, 2B). The best-fit curves (shown in fig. 2A) show that ω increases from minimally vegetated- to vascular plant- to angiosperm-worlds within generations of climate model experiments, although the specific values of ω differ greatly (fig. 2A; table 2). In addition to using climate model simulations, we also use a compilation of direct, hydrological measurements (Bosch and Hewlett, 1982; Brown and others, 2005) at paired watersheds that compare vegetated vs. non-vegetated (that is, clear-cut) treatments (irrespective of plant composition). These modern vegetated (both angiosperm and gymnosperm-dominated) watersheds have higher *ET* relative to their paired, clear-cut counterparts (fig. 2B). To estimate ω from these paired watersheds, we combine estimates of E_p (Trabucco and Zomer, 2009) with the observed change in runoff. The vegetated catchments have a ω value of 2.6, which is in concordance with estimates from larger datasets of modern catchments (Greve and others, 2015), whereas clear-cut, non-vegetated sites are characterized by a lower ω value of 1.9 (fig. 2B). Based on these constraints from our Budyko analysis, we select a range of values to represent end-member scenarios for minimally vegetated (ω = 1.5; fig. 1 upper panels), and angiosperm (ω = 2.5; fig. 1 lower panels) worlds, with an intermediate value representing the vascular plant world (ω = 2.2). As a sensitivity test, we also present a broader range of ω values in our analysis from no evapotranspiration (ω = 1.0) to highly optimized inland vapor recycling (ω > 3.5). As such, our modeling is intended to capture the direction and trends in weathering, despite uncertainties in constraining ω.

Effect b: Local Water Vapor Recycling (f) Through the Depth of Plant Rooting

Two key, coupled changes for hydrologic cycling are induced by the evolution of deep-rooted plants. First, because plants increase ω, both *ET* and *P* increase, resulting in greater recycling of precipitation (Kleidon and others, 2000; Boyce and Lee, 2010, 2011; Alkama and others, 2012). Second, this recycled precipitation can more fre-

A. Climate Models

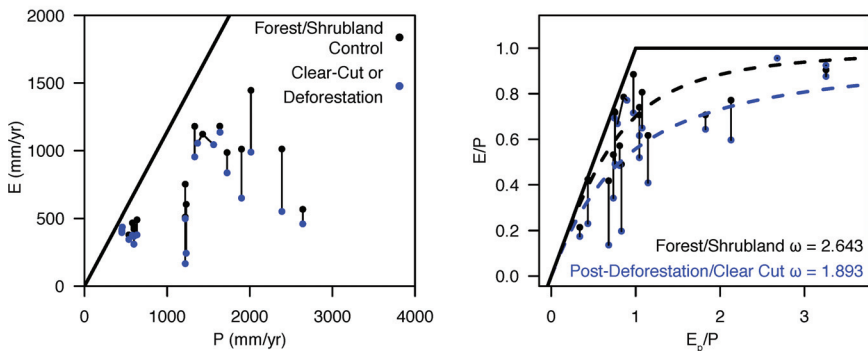## Boyce and Lee (2010) NCAR CAM3.0/CLM 3.5

Fig. 2. Determination of the effect of plants on water fluxes in Budyko space. (A) Climate model simulations from Boyce and Lee (2010) (see also Lee and Boyce, 2010; Lee and others, 2012) using NCAR CAM3.0/CLM 3.5. Each land grid cell is represented by a gray dot. Net irradiance (R_{net}) is the sum of incoming and outgoing longwave and shortwave radiation and can be equated with potential evapotranspiration, E_p, (for explanation see Roderick and others, 2014), which was then converted into water units using the latent heat of vaporization for water. Black dots are the binned average ET/P for every increment of 0.25 R_{net}/P, and the black line is the best-fit line to the binned averages (see reasoning in Koster and others, 2006). Note that in the no transpiration case there are less land points shown because they either violate mass balance (E>P) and were not included, or sit to the right ($R_{net}/P > 3$) of the axes shown. (B) Compilation of field experiments of deforestation or clear-cutting where the necessary climatological parameters are available to assess the impact of decreased transpiration (see compilation in table A2). The modern observation of ω (2.643) agrees well with the median value from Greve and others (2015), which analyzed more than 400 modern catchments. Budyko curves were fit using the 'nls2' R package (Grothendieck, 2013).

quently transit the entirety of the weathering zone without entering runoff due to the presence of deep-rooted vascular plants that can draw upon deep water for transpiration. Consequently, a fundamentally new weathering-zone dynamic appears after the colonization of land by plants whereby water availability in the weathering zone may no longer be strictly delineated by runoff, but also by the frequency with which water is recycled through the weathering zone (Drever, 1992).

To account for deep-rooted vascular plants, we modify equation 5 in Model 2 and add a recycling factor (f):

$$C = C_{max} \frac{f\tau Dw/q}{1+f\tau Dw/q}. \tag{7}$$

Here, the recycling factor (f) is the ratio of precipitation to runoff (P/q). This form of the equation applies to a situation in which plant roots extend to or beyond the actively weathering zone (that is, near the soil-saprolite-bedrock interface)—such as large trees do today (Stone and Kalisz, 1991; Ehleringer and Dawson, 1992; Jongmans and others, 1997; Landeweert and others, 2001; Lucas, 2001). In this scenario, the transpired water moves through the weathering zone but does not enter runoff and instead would be recharged to the atmosphere (green ET arrow in lower right panel of fig. 1), effectively increasing the residence time of each water parcel in each grid cell as vapor is transported into the continental interior. Thus, equations 5 (*sans* recycling factor) and 7 represent two end-members that mimic a shallow rooting versus a deep rooting environment.

Since f is calculated for every grid cell of the domain, and thus evolves spatially along the continental transect, this formulation satisfies the observational and modeling evidence (primarily from precipitation stable isotope measurements and analyses of wind and humidity gradients) that downstream recycling is important, particularly in inland continental settings such as Eurasia and southern Africa today (Salati and others, 1979; Brubaker and others, 1993; van der Ent and others, 2010; Caves and others, 2015; Bershaw, 2018). For example, an analysis of atmospheric convergence by Brubaker and others (1993) found that the local contribution from recycled evapotranspiration to monthly precipitation in many regions accounts for up to 40 percent of precipitation; in Central Asia, this percentage may reach beyond 80 percent (van der Ent and others, 2010). Additionally, both atmospheric vapor content and hence continental vapor recycling increase in the simulations (Boyce and Lee, 2017; Lee and Boyce, 2010; Boyce and Lee, 2010, 2011) that are used to parameterize Model 1. Our specific formulation for incorporating the appearance of deep-rooted plants may not precisely capture the complex dynamics that occur between precipitation, rooting-depth, and soil moisture; nevertheless, we view equation 7 as a first-order attempt to capture a fundamentally novel switch between a shallow-rooted, low recycling world and a deep-rooted, high recycling world.

Effect c: Enhancement of Chemical Weathering Reactions Through Productivity

In addition to generating a more active terrestrial hydrological cycle, plants also increase the thermodynamic limits of chemical weathering reactions. This effect has been shown by previous studies that emphasize the effects of plants on precipitation, soil moisture, and primary productivity, which affect soil pCO_2 and thus chemical weathering reactions (for example, Berner, 1992; Drever, 1994; Kelly and others, 1998). In our model framework, these effects are encapsulated in the C_{max} term (Model 2; eqs. 5 and 7)—the thermodynamic maximum weathering solute concentration as determined by soil conditions. We carried out equilibrium reaction path simulations to calculate C_{max} from weathering of granitic bedrock to secondary aluminosilicate minerals as a function of soil pCO_2 with the "React" module of The
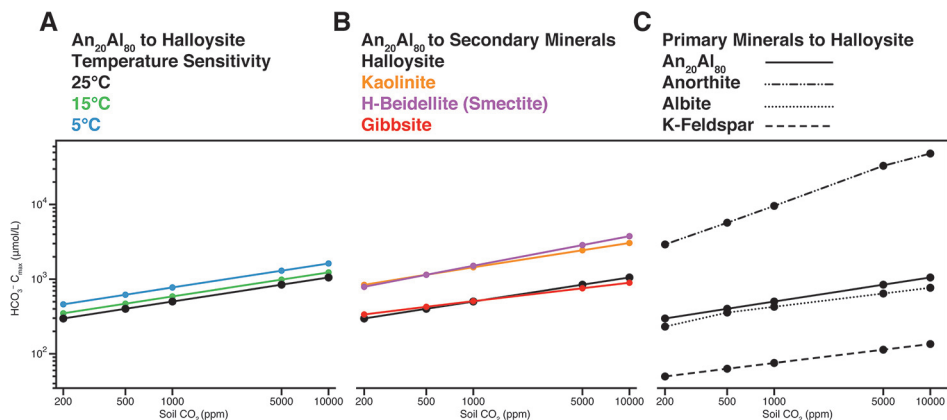
Fig. 3. Results of GWB titration experiments (Bethke, 2007) reacting rainwater (see Maher and others, 2009) with feldspars to form secondary minerals to determine C_{max} values of HCO_3^-. Batch calculations were carried out to completion at a fixed fugacity of pCO_2 (that is, an infinite reservoir) to explore the effect of temperature (left panel), secondary mineral end-member, and primary mineral starting material.

Geochemist's Workbench (GWB; Bethke, 2007). The following standard states were adopted for the thermodynamic calculations: unit activity for pure minerals and H_2O at any temperature and pressure; for aqueous species, unit activity of the species in a hypothetical 1 mol/kg solution referenced to infinite dilution at any temperature and pressure; for gases, unit fugacity of a hypothetical ideal gas at 1 bar of pressure. Soil pCO_2 and fugacity are related by the fugacity coefficient, λ, by $fCO_2 = \lambda \times pCO_2$. Similarly, C_{max} is obtained from the aqueous species concentration (μmol/l) of HCO_3^- as the weathering solute representative of silicate weathering, which is related to activity through the activity coefficient, γ, by $a = \gamma \times C$. Thermodynamic data is from the Thermoddem database (version llvl2; Blanc and others, 2012).

Using a fixed fugacity of CO_2 representing an open system with an infinite reservoir of CO_2, pH was determined by charge balance and allowed to evolve over the course of the reaction. An initial mineral phase of Na-rich plagioclase ($An_{20}Al_{80}$, 20 mol% anorthite and 80 mol% albite) was added to water for a fluid:rock ratio of 100. The secondary mineral phase allowed to precipitate was the hydrated aluminosilicate halloysite ($Al_2Si_2O_5(OH)_4$). This reaction is

$1.67An_{20} + 3H_2O + 2CO_2$ (aq) =

$$\text{Halloysite} + 1.33Na^+ + 2.67SiO_2(aq) + 0.33Ca^{2+} + 2HCO_{3^-} \quad (8)$$
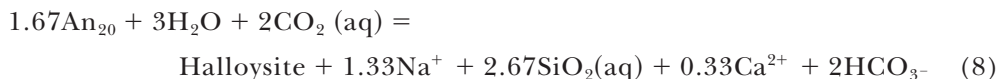
We perform this calculation across a wide range of soil pCO_2 (200–10,000 ppm). The CO_2 (aq) is set to be in equilibrium with the specified pCO_2 at the given temperature. To test the sensitivity of our calculations to different primary and secondary mineral phases and to temperature, we vary the composition of the initial feldspar in equation 8, the secondary mineral phase, and the reaction temperature (5–25 °C). The initial water composition is from Maher and others (2009) (see their Table 2) and is representative of dilute rainwater. Note that the simulations shown here using GWB are analogous to the 'open-system' soil column reactive transport simulations presented by Winnick and Maher (2018) (see their Figure 3).

Several results follow from this analysis and confirm previous modeling (Maher, 2011; Maher and Chamberlain, 2014; Ibarra and others, 2016; Thomas and others, 2016; Winnick and Maher, 2018). First, these calculations show that in all cases, HCO_3^-

and $SiO_2(aq)$ C_{max} values will increase with increasing soil CO_2 regardless of parent material, reaction temperature, or specific clay forming reaction (fig. 3). Second, the C_{max} values are relatively insensitive to temperature over reasonable Earth surface values (fig. 3A) (as previously shown by Maher and Chamberlain, 2014; Winnick and Maher, 2018). Third, the C_{max} values are relatively sensitive to the specific soil forming reaction and parent material (figs. 3B and 3C). For example, we use the reaction that forms halloysite (following Maher, 2011; Maher and Chamberlain, 2014) because it results in HCO_3^- and $SiO_2(aq)$ C_{max} values in close agreement (factor of 2 to 10 scaling) with modern solute data (Drever and Zobrist, 1992; Arthur and Fahey, 1993; Berner and Rao, 1996; Bormann and others, 1998; Moulton and Berner, 1998; Gaillardet and others, 1999; Moulton and others, 2000; Maher and Chamberlain, 2014; Ibarra and others, 2016, 2017; Wymore and others, 2017). This reaction estimates the lowest values of C_{max} for a given soil CO_2 (fig. 3), whereas using kaolinite as the secondary mineral predicts much higher values of C_{max}. Using Na-rich plagioclase feldspar An_{20}/Al_{80} gives intermediate C_{max} values between that of weathering of potassium feldspar (lowest C_{max}) versus pure anorthite (highest C_{max}). Critically, our sensitivity analysis shows that the slopes of the relationship between soil CO_2 and C_{max} for different primary and secondary minerals are very similar (with the exception of 100% anorthite as the primary mineral). Thus, although the absolute C_{max} value for each scenario may depend on the assumed generalized reaction stoichiometry, the change in C_{max}—and therefore the effect of plants on weathering—as soil CO_2 increases is not sensitive to the reaction chosen.

In addition to using GWB simulations, we also compare to data from Moulton and Berner (1998) (as well as Moulton and others, 2000; Oskarsson and others, 2012) that compared weathering fluxes from a barren (minimally vegetated) and a vegetated basaltic catchment in Iceland. We use the distribution of concentration measurements and calculate the 95 percent maximum (percentile) of the data (fig. 4) to estimate C_{max} values (following Dixon and von Blanckenburg, 2012; Maher and Chamberlain, 2014; Ibarra and others, 2016). We find that the C_{max} values increase ~1.8-fold between barren and vegetated catchments, in agreement with the range suggested by our GWB simulations, although Iceland soil pCO_2 for the catchments studied by Moulton and Berner (1998) are unknown and represent relatively low C_{max} concentrations relative to a synthesis of modern basaltic catchments (Ibarra and others, 2016).

Because C_{max} is sensitive to soil pCO_2 and soil pCO_2 is sensitive to climate (Cotton and Sheldon, 2012; Oskarsson and others, 2012; Montañez, 2013), we vary C_{max} across our continental transect as a function of precipitation. That is, C_{max} is allowed to evolve (decrease) laterally across the domain as precipitation rates decrease due to the loss of water as runoff. To provide C_{max} estimates for each grid cell on our continental transect, we first calculate soil pCO_2 as a function of precipitation using data compiled by Cotton and Sheldon (2012) and Cotton and others (2013), which show that soil pCO_2 is positively correlated with precipitation for the mid-latitude sites they examined, primarily in western North America (see fig. A4). We note that, particularly in semi-arid midlatitude sites, there are large seasonal variations in soil CO_2 (Breecker and others, 2009; Oerter and Amundson, 2016), however, given the steady-state nature of our calculations, we are unable to account for seasonal fluctuations. Further, weathering likely occurs during the period when precipitation occurs, which is correlated with increasing productivity and hence higher soil pCO_2. Using the regression shown in figure A4, we calculate how C_{max} of HCO_3^- varies with soil pCO_2, assuming that C_{max} varies between approximately 250 μmol/L in low soil pCO_2 (200 ppm) locations to approximately 1200 μmol/L in high soil pCO_2 environments using a regression between the reaction path C_{max} of HCO_3^- results and the simulated soil pCO_2 values (fig. 3, solid black line in each panel; fig. A4). As discussed above, this
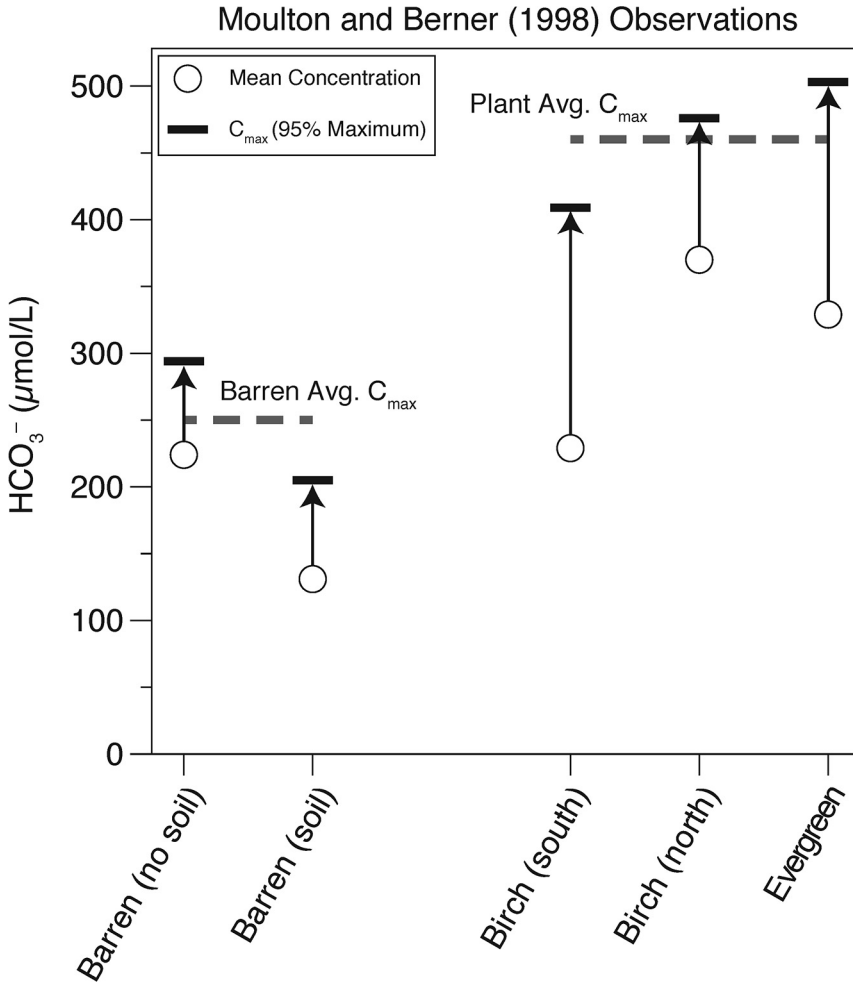
Fig. 4. Summary of stream concentration data by Moulton and Berner (1998) for barren (minimally vegetated) and vegetated modern landscapes. Following previous work (Dixon and von Blanckenburg, 2012; Maher and Chamberlain, 2014; Ibarra and others, 2016), C_{max} is calculated assuming the 95% maximum (horizontal black lines) calculated from the mean concentrations (white dots) and observed distributions (Table 1 of Moulton and Berner, 1998). Average values are taken for C_{max} values for plant and barren landscapes (dashed lines).

relationship is in qualitative agreement (in direction and magnitude) with the Moulton and Berner (1998) observations.

Modeling Setup and Assumptions

Our modeling is a simplified representation of how plants impact chemical weathering and the hydrologic cycle. As a result, we have made several key assumptions that may limit the potential for this work to be scalable to global weathering relationships. The limitations of this modeling setup include:

1) Vapor transport and land surface-atmosphere exchange is constrained to follow the Budyko curve formulation. While representative datasets spanning different climates (for example Koster and others, 2006; Greve and others,

2015) and climate model experiments (for example Roderick and others, 2014; see also fig. 2) follow Budyko landscape parameters (ω values) centered on ~2.6 today, continental transects as simulated in our model do not necessarily follow this trend. In fact, some evidence from the mid-latitudes suggests lower ω values in mountainous continental interiors (see Greve and others, 2015).

2) Ocean evaporation and thus the flux into the domain is held constant as prescribed by the constant flux boundary condition. This flux may change in response to the biophysical effects of plant evolution, including changes in albedo and surface roughness, which we do not consider in this study. Nevertheless, this boundary condition and consequent model results are supported by a climate model (whose results are utilized here; from Boyce and Lee, 2010): despite predicting a slight decrease in global runoff, this model also predicts significant changes in precipitation patterns with changing plant transpiration.

3) The two models are calibrated to, and thus representative of, a mid-latitude continent-dominated world for two reasons. First, we have chosen a Peclet number of 1 (see above) for the vapor transport module, which influences the degree of rainout and advection of moisture inland. Second, in modern mid-latitude settings, many surfaces are young and not 'supply limited'. This is important because flat tropical environments today produce some of the lowest area-normalized weathering rates despite high precipitation and runoff due to thick regolith (weathering zone) development in humid, tropical regions (for example, West and others, 2005; Godderis and others, 2006; Hewawasam and others, 2013).

Future work that extends our results may include coupling global climate model output (for example, Boyce and Lee, 2017) with weathering fluxes (for example von Blanckenburg and others, 2015), or directly modeling the influence of plants on transpiration and weathering reactions in intermediate complexity models (such as cGENIE; Colbourn and others, 2015).

MODEL RESULTS

We find that the impacts of plants agree well with previously estimated effects of plant evolution on weathering; however, our model framework allows us to calculate how this cumulative effect is partitioned between hydrologic vapor recycling effects and thermodynamic effects. Our results support the hypothesis that plants will increase the areal distribution over which precipitation – and hence chemical weathering – occurs as vapor is recycled downwind. Due to only this hydrological change, we estimate that the colonization of vascular plants over a minimally vegetated world will increase solute concentrations by approximately a factor of 1.6 for a fixed atmospheric CO_2 concentration. Further, we attempt to quantify the increase in chemical weathering due to plant/rock/groundwater interactions in the weathering zone. Our model demonstrates that this feedback plays a significant role in increasing weathering solute concentrations, potentially by a factor of about 1.5. Finally, we calculate that the evolution of angiosperms, depending on the efficiency of hydrologic recycling effects and thermodynamic effects by gymnosperms, increased weathering concentrations by an additional 7 to 55 percent.

Continental Transects of Hydrology and Weathering

Our calculations of the role of vapor transport by plants (Model 1) show that plants significantly increase the areal extent over which precipitation occurs over continents. In figure 5, we show simulations using ω values representative of no transpiration (minimally vegetated world; ω = 1.5), non-angiosperm vascular plants
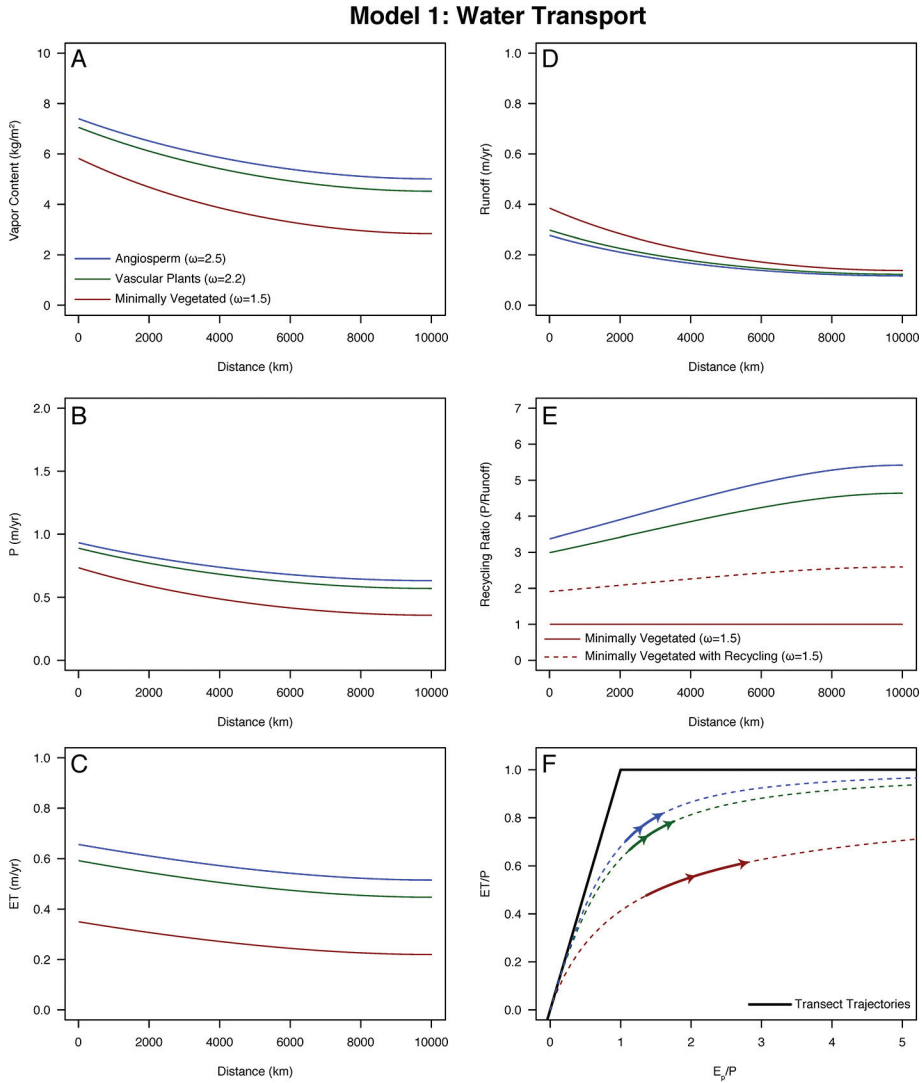
Model 1: Water Transport

Fig. 5. Water fluxes simulated by Model 1 using constant flux (left-hand boundary) to constant gradient (right-hand boundary) boundary conditions (see fig. 1 and text for explanation). Results show ω values representing the simulations from Boyce and Lee (2010) and modern observations as in figure 2. (A) Total water vapor content, (B) precipitation, (C) evapotranspiration, (D) runoff, (E) recycling ratio (P/runoff) and (F) the evolution of the vapor transport profiles in Budyko space.

(ω = 2.2), and modern angiosperms (ω = 2.5) (table 2). As shown in figure 5, water vapor content in the atmosphere, precipitation, and evapotranspiration increase at each transition from a minimally vegetated landscape to a vascular plant world and to an angiosperm world. The effect of water replenishment of the atmosphere by evapotranspiration (fig. 5C) leads to a flatter distribution of runoff along the moisture transport pathway in both the vascular plant and angiosperm worlds (fig. 5D). Total runoff decreases relative to a minimally vegetated world by 17 percent and 23 percent, respectively. Additionally, at any point along the continental transect, the land surface has a greater recycling ratio in plant covered landscapes, with a greater effect for
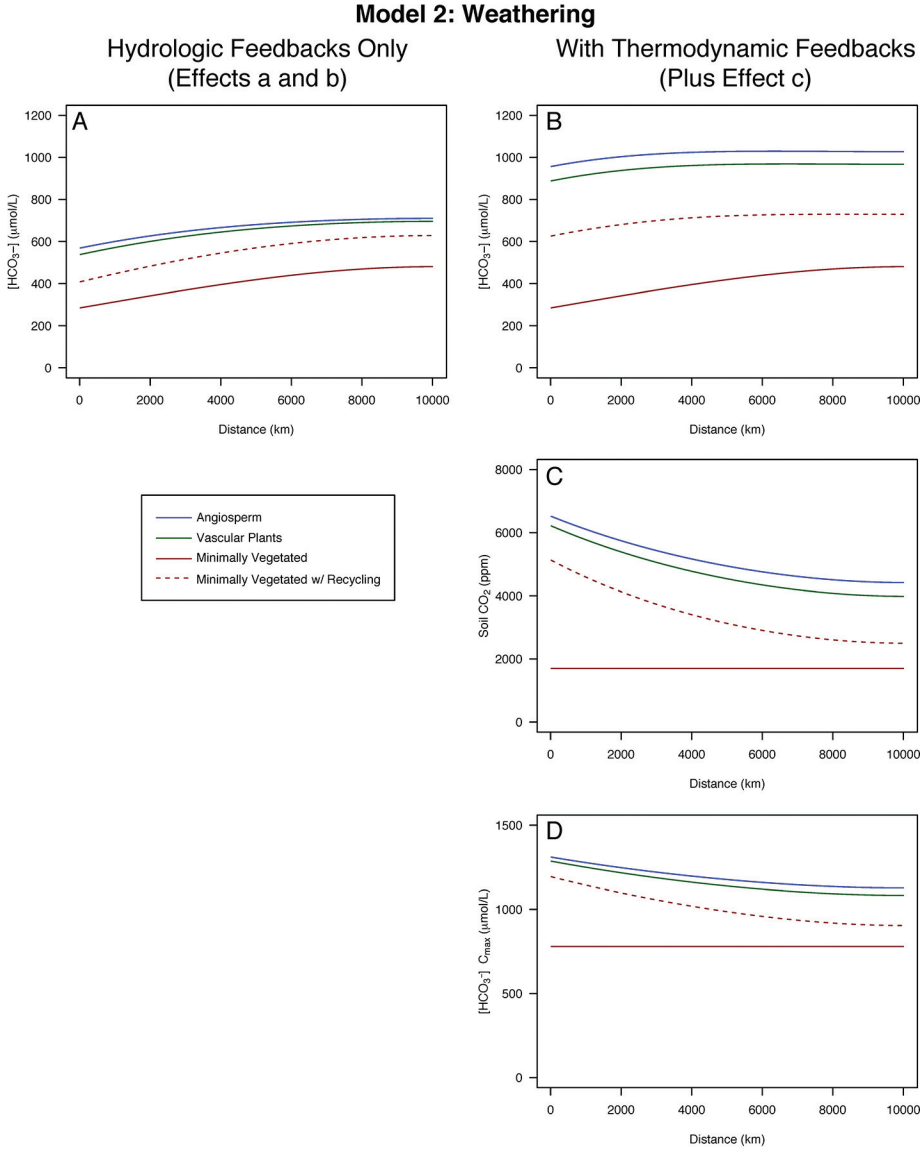
Model 2: Weathering

Fig. 6. Solute fluxes simulated by Model 2 using inputs from Model 1 (fig. 5). (A) Solute $[HCO_3^-]$ with hydrologic feedbacks (effects a and b) only. Lines correspond to A, A', B' and C' in figure 7 (middle and left panels). Soil pCO_2 and C_{max} $[HCO_3^-]$ are invariant when only hydrologic feedbacks are included. (B) Solute $[HCO_3^-]$; (C) soil pCO_2; (D) C_{max} $[HCO_3^-]$ including both hydrologic and thermodynamic feedbacks. Lines correspond to A, A'', B'', and C'' in figure 7 (right and left panels).

angiosperms than for gymnosperms (fig. 5E). Together, these results show that the hydrologic cycles in minimally vegetated-, in vascular plant-, and in angiosperm-worlds are distinct (fig. 5).

In figure 6, we show how weathering-related parameters change across the continental transect as a function of hydrologic changes alone (panel A; effects a and b) or as a function of both hydrologic changes and thermodynamic feedbacks (panels

Summary of model results and GEOCARBSULF parameters based on Berner (2006) and Royer and others (2014)

	Norm. runoff	C_{max} [HCO$_3^-$] (µmol/L)	f_{avg}	[HCO$_3^-$] (µmol/L)	Norm. [HCO$_3^-$] (µmol/L)	[HCO$_3^-$] (µmol/L)	Norm. [HCO$_3^-$] (µmol/L)
Constant Flux to Constant Gradient Boundary Conditions							
	Figures 5 and 6 Curves			Figure 7 (Effects a and b)		Figure 7 (Effects a, b and c)	
Minimally Vegetated with No Recycling Feedbacks (ω=1.5)							
Dw = 0.03	1	779	1	387	1.00 (A)	n/a	n/a
Minimally Vegetated with Recycling Feedbacks (ω=1.5) vs. Minimally Vegetated (ω=1.5)							
Dw = 0.03	1	1035	2.246	530	1.37(A')	697	1.80(A'')
Vascular Plants (ω=2.2) vs. Minimally Vegetated (ω=1.5)							
Dw = 0.03	0.826	1125	3.833	633	1.64(B')	927	2.39(B'')
Angiosperm (ω=2.5) vs. Minimally Vegetated (ω=1.5)							
Dw = 0.03	0.775	1215	4.423	655	1.70(C')	986	2.55(C'')
GEOCARBSULF Weathering Sensitivities (Berner, 2006; Royer and others, 2014)							
	Mean	2σ Range				Mean	2σ Range
Minimally Vegetated vs. Angiosperm (LIFE)	0.250	0.125 to 0.325		Angiosperm vs. Minimally Vegetated		4.0	2.0 to 6.0
Vascular plant vs. Angiosperm (GYM)	0.875	0.459 to 1.291		Vascular plant vs. Minimally Vegetated		3.5	1.1 to 5.9

All values normalized to minimally vegetated ($\omega = 1.5$) minimum weathering flux (Dw = 0.03 m/yr; soil CO$_2$ = 1700 ppm), which corresponds to point A on figure 7. Letters correspond to points on figure 7 and curves on figure 6. All values given for Dw = 0.03 m/yr. Norm. – Normalized.

B, C and D; effects a, b and c). *Dw* values, a measure of the reactivity of the weathering zone, are held at 0.03 m/yr in figure 6 (global average determined by Maher and Chamberlain, 2014). In a minimally vegetated world, soil pCO$_2$ remains low (1700 ppm) relative to highly productive soils (10,000 ppm; Cotton and Sheldon, 2012; Montañez, 2013; Cotton and others, 2013) and is unchanged by precipitation because the deep soil expression of plant productivity is only weakly (or not at all) responsive to changes in precipitation. Soil pCO$_2$ for the minimally vegetated world is estimated to be 1700 ppm from reconstructions of Cambrian and early Ordovician atmospheric pCO$_2$ levels (Yapp and Poths, 1992; Mora and others, 1996; Foster and others, 2017), though we note that there is evidence for soil pCO$_2$ elevated above atmospheric levels in pre-vascular plant soils (Yapp and Poths, 1994). In contrast, for all plant scenarios, soil pCO$_2$ scales with precipitation (following the above described modeled relationships), with higher soil pCO$_2$ near the coast and lower inland (fig. 6C). We also show a minimally-vegetated world with soil pCO$_2$ scaling with precipitation (red dashed lines in fig. 6).

Bicarbonate C_{max} values, which are scaled to precipitation, follow soil pCO$_2$ (fig. 6D) and decrease inland, while [HCO$_3^-$] increases inland (fig. 6B). Increasing [HCO$_3^-$] inland results from decreasing q from the coast to the interior. Consequently, the concentration of weathering solutes approach C_{max} values at low runoff because of less dilution (Maher and Chamberlain, 2014; Ibarra and others, 2016; Wymore and others, 2017). This increase is also smaller when only hydrologic feedbacks (effects a and b) are included (fig. 6A), accounting for 43 percent of the increase in both the gymnosperm and angiosperm cases (table 3). If total runoff

across the domain is held constant, using constant flux to constant flux boundary conditions, the trends and magnitude of concentration change are comparable (see fig. A5, panel F).

Sensitivity to Changes in ω *and Dw*

The results presented in figures 6 and 7 show the cumulative impacts of global hydrologic change and local thermodynamic effects on solute concentrations.

The effect of increased distribution of precipitation by plants (that is, plant recycling feedbacks) on weathering solute concentrations is shown in figure 7 (represented by ω values on y-axis). Here, for any given bedrock weathering zone (represented by varying Dw), $[HCO_3^-]$ increases from minimally vegetated to angiosperm worlds. The absolute value of this effect is strongly dependent upon the erosional regime, which is encapsulated by the Dw value (x-axis of fig. 7). All concentration values on both panels are normalized to the case of a minimally vegetated world with global average Damköhler coefficient values (ω = 1.5, Dw = 0.03 m/yr). In the left panel of figure 7, showing our results without plant recycling feedbacks, average soil weathering concentrations are primarily set by the Dw values (x-axis), with minimal sensitivity to ω values. Values increase slightly with increasing ω due to flattened runoff gradients (fig. 5D) leading to higher weathering concentrations closer to chemostatic concentrations.

Inclusion of plant recycling feedbacks dampens the response to Dw values and amplifies the model response to ω. Moving from point A to point A' in figure 7 represents addition of plant recycling feedbacks only (effects a and b with introduction of the recycling term, f, in eq. 7) and results in a 1.37-fold increase in weathering concentration (see also table 3). Moving from point A' to B' to C' on figure 7 (middle panel) represents increasingly efficient recycling as ω increases. Further, the effect of increasing recycling and precipitation rates on global-scale recycling feedbacks, along with local-scale feedbacks increasing soil pCO_2 (fig. 6C), results in a slight decrease in the effective Dw values due to increases in C_{max} (fig. 6D). This is because C_{max} also appears in the denominator of Dw (see eqs. 5–7), which is represented by the trajectory of points A to A'' to B'' to C'' in the right panel of figure 6, where $[HCO_3^-]$ concentrations increase 2.39 (point B'') and 2.55 (point C'') fold. If the effect of C_{max} on the denominator of Dw is not accounted for, this would lead to minimal overestimation (a few percent) of the weathering concentration increases (see contours of Dw and ω relative to points B'' and C''). However, if plants also increased the length scale (deeper soils) represented by increased Dw values, these weathering concentration changes may be greater. For example, for modern mountain Dw values of 0.3 m/yr (Maher and Chamberlain, 2014), vascular plant-world weathering solute concentrations would have increased by a factor of ~2.8, with angiosperm-world concentrations increasing to a factor of ~3.0 (all relative to the minimally vegetated world; fig. 7, right panel). Thus, the magnitude of increased weathering solute concentrations depends upon whether these changes occur in low-relief cratonic areas versus highly erosional mountainous regimes, the paleogeography of those mountainous regions, and exposed continental area as influenced by sea level or continental freeboard changes. Increased inland vapor recycling increases the likelihood that precipitation reaches inland cratonic mountain ranges. Regardless of topography, each transition in plant evolution increased the thermodynamic potential for solute generation by increasing soil pCO_2 (C_{max}), increased vapor recycling (f), and possibly by deepening the soil weathering length scale (Dw).

Uncertainty of the Calculations

There is significant potential uncertainty in our calculations related to both changes in the Budyko landscape parameter (ω values) and potential effects due to
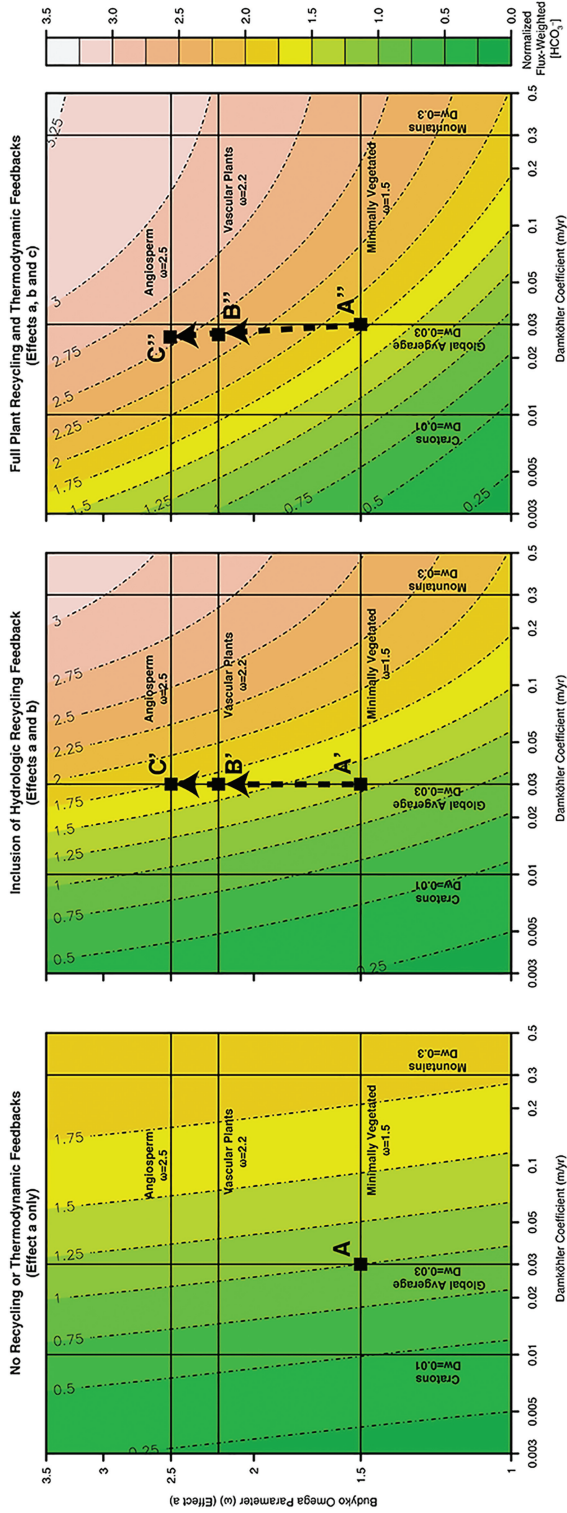
Fig. 7. Contour plots of weathering concentration (flux weighted) for varying values of D_W and ω. All weathering concentrations are normalized to the minimum vegetation scenario (point A on left panel) with no plant recycling feedbacks ($D_W = 0.03$ m/yr; $\omega = 1.5$, $C_{max} = 1700$ ppm; see text for details). Points correspond to curves in figure 6: A – minimally vegetated, A' – minimally vegetated with recycling, B' – vascular plants with recycling, C' – angiosperms with recycling, A'' – minimally vegetated with recycling and thermodynamic effects, B'' vascular plants with recycling and thermodynamic effects, and C'' angiosperms with recycling and thermodynamic effects. Black arrow trajectories show increases in both local effects and global effects of increased downstream vapor recycling.

temperature on the maximum weathering concentration (C_{max}). The fits to the climate model fluxes shown in figure 2 have an uncertainty (standard error for ω values) of ± 0.02 to 0.09. The maximum uncertainty value of 0.09 propagates to a ~10 percent uncertainty in the calculated concentration changes (points A', B' and C') when only effects a and b (the hydrologic effects) are accounted for (see blue dots in fig. A6).

Uncertainty due to temperature effects on the thermodynamics of the net weathering reaction are explored in figure 3A. While the slope does not change, the absolute value of the C_{max} values increase with lower – or decrease with higher – temperatures, as recently shown using similar reactive transport simulations by Winnick and Maher (2018). Because the thermodynamic rate constants are non-linear for the net weathering reactions (see Maher and Chamberlain, 2014), the uncertainty is asymmetric. Propagating the range of C_{max} values determined for 5 and 25 °C, relative to the GWB simulations at 15 °C, give an uncertainty of 31 percent and 15 percent, respectively, when accounting for all effects (both thermodynamic and dynamic) (see green dots in fig. A6; points A'', B'', and C''). As such, our calculations are more uncertain at colder temperatures (lower atmospheric CO_2).

Analysis of the cumulative uncertainties associated with only hydrologic effects and both hydrologic and thermodynamic effects (fig. A6), shows that our vascular plant- and angiosperm-worlds are significantly different from a minimally vegetated world (even with the inclusion of all recycling effects). However, for changes due to only hydrologic effects (blue dots; points B' and C'), the change in weathering solute concentration is not significantly different between our vascular plant and angiosperm-worlds because the Budyko ω values are relatively similar (2.2 and 2.5, respectively), leading to similar runoff distributions (fig. 5D). Nonetheless, when all effects are considered (green dots; points B'' and C'') changes in weathering concentration are distinct between our vascular plant- and angiosperm-world concentrations, with the lower bound of the angiosperm concentration (C'') approximately equal to the average value for the vascular plant concentration (B'').

DISCUSSION

Plant Evolution and Weathering

As illustrated by the modeling results presented in this study, the evolution and spread of land plants enhanced chemical weathering concentrations through two complementary mechanisms: *(1)* increasing the down-wind transport and recycling of precipitation; and, *(2)* increasing the thermodynamic maximum of solutes (C_{max}) produced from weathering via an increase in soil pCO$_2$. The ability of a continental surface to generate higher solute concentrations means that the weathering flux should be higher at any given runoff. However, the globally averaged silicate weathering flux must equal the volcanic and metamorphic flux of carbon on geologic (that is, 1 Ma) timescales (Berner and Caldeira, 1997; Broecker and Sanyal, 1998; Zeebe and Caldeira, 2008; Caves and others, 2016a). Consequently, a world populated with plants in which the efficiency of weathering increases requires a reduction in other factors which contribute to weathering, such as atmospheric CO_2 concentrations, temperature, and runoff. Consequently, each step in plant evolution may permit a lower steady-state atmospheric pCO$_2$, resulting in lower steady-state temperature and therefore runoff. Further, that weathering solute concentrations are higher in a world with plants indicates that sudden increases in runoff—driven perhaps by large carbon cycle perturbations—will produce correspondingly larger increases in the weathered solute flux and thus a more rapid reduction in temperature and runoff. Thus, we suggest that the strength of the silicate weathering feedback increased as plants colonized the continents and the largest increase is the result of deep rooting vascular plants in

the late Devonian and Carboniferous, with a somewhat smaller increase during the expansion of angiosperms in the Cretaceous and Cenozoic.

The effect of plants on chemical weathering were qualitatively outlined by Berner (1992) and Drever (1994) and quantitatively incorporated into the GEOCARB family of models, most recently GEOCARBSULF (Berner, 2006; see also more detailed model description in Berner and Kothavala, 2001 and Royer and others, 2014, as well as incorporation into COPSE in Bergman and others, 2004). To incorporate the many possible mechanisms for enhanced weathering by plants (Berner, 2006), these models treat the effect of plants on weathering such that: 1) pre-Devonian weathering rates are 25 percent as sensitive to changes in pCO$_2$ compared to modern weathering rates; 2) the effect of gymnosperms begins at 380 Ma and ramps up to full vascular plant effect at 350 Ma with weathering rates 87.5 percent as sensitive compared to modern; and 3) angiosperm weathering sensitivity is the same as modern weathering rate sensitivity and ramps up over the period from 130 to 80 Ma (see Berner and Kothavala, 2001; Royer and others, 2014; summarized in table 3). Of similar magnitude, steady-state mass balance calculations from the GEOCLIM model (Donnadieu and others, 2006, 2009; Le Hir and others, 2011) suggest increases in silicate weathering in the late Devonian decreased atmospheric pCO$_2$ by a factor of 1.55. Additional effects of plant weathering have often been incorporated by a CO$_2$ fertilization of productivity term that averages across the variability in response seen in the modern vegetation (Mooney and others, 1991; Berner, 1994; Banwart and others, 2009), although applicability to the non-angiosperm fossil record has been questioned (Boyce and Zwieniecki 2012). However, CO$_2$ fertilization of productivity is not considered in the modeling performed here.

In a broad sense our results are similar to previous estimates, with some key differences. Before discussing these differences, it is important to note that our estimates of weathering rate changes depend upon: 1) where on the landscape weathering occurs (for example, mountains versus lowlands, which influences *Dw*); 2) the estimated Budyko dimensionless landscape parameter (ω) in equation 4, which determines the conversion efficiency of *P* to *ET* for vascular plant and angiosperm worlds; 3) whether water is recycled through the entire weathering zone or only part of it; and, 4) the spatial extent of deep rooting plant cover.

The enhanced movement of water across the landscape due solely to increased transpiration has minimal impact on weathering directly; the key is the repeated interactions with the substrate that this transpirative recycling affords (represented by moving vertically in the fig. 7 panels). Water vapor can be recycled such that water does not immediately enter runoff and instead can enter the weathering zone again through transpirative return of water to the atmosphere if rooting depth of plants occurs near (or below) the depth of the weathering front (for example, Stone and Kalisz, 1991). Our results support past recognition that inland transpiration recycling can even decrease total runoff amount overall as water is lost as vapor off the downwind side of the continent (Kleidon and others, 2000; Alkama and others, 2012) (fig. 5D). With our preferred boundary conditions (constant flux to no gradient) and calibrated ω values (fig. 2), runoff decreases by 17 percent and 23 percent for the vascular plant- and angiosperm-worlds, respectively, relative to the minimally vegetated scenario (fig. 5D, integral of green and blue curves relative to red curve).

Many individual plants have relatively shallow roots. As such, the focus here on water being entrained into transpiration only after it has already participated in weathering is an end-member case, but a reasonable one. The critical part of the weathering zone—where the most solute is generated, the most CO$_2$ is converted to alkalinity, and primary minerals are depleted and secondary minerals precipitated—tends to be in the zone of seasonal water table fluctuations, particularly in low-lying areas (Stone and Kalisz, 1991; Ehleringer and Dawson, 1992; Jongmans and others,
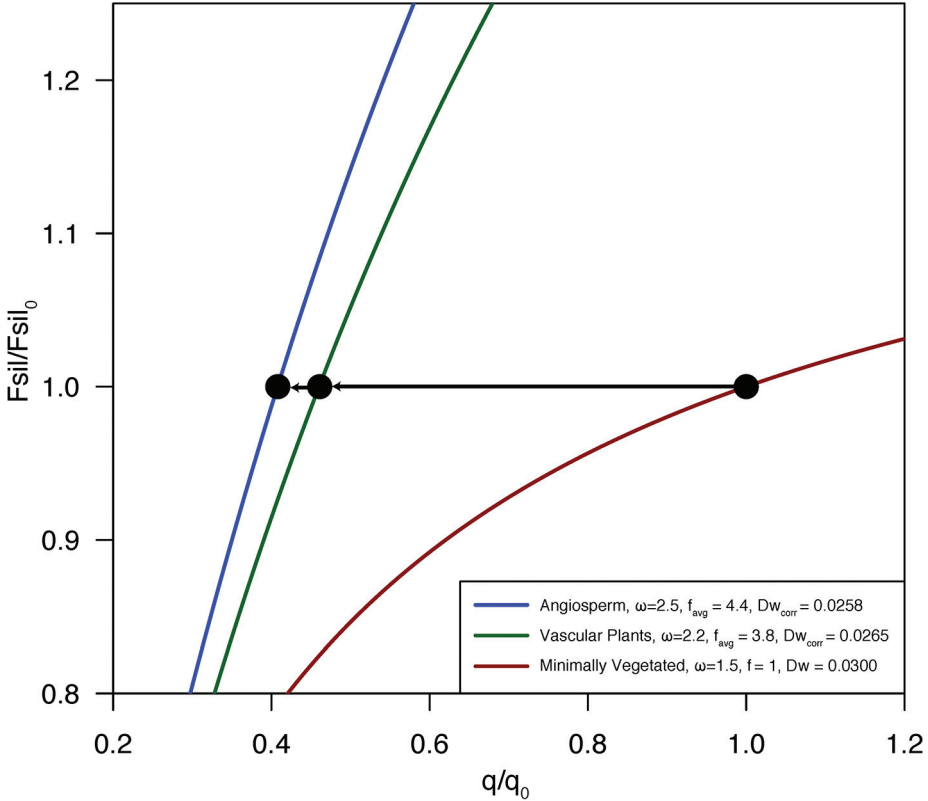
Fig. 8. Sensitivity of weathering fluxes (F_{sil}) to perturbations in climate, through changes in runoff (q), using framework presented in this paper (after Maher and Chamberlain, 2014; von Blanckenburg and others, 2015; Ibarra and others, 2016). All lines are plotted for the global average Damköhler coefficient ($Dw = 0.03$ m/yr) adjusted for increased C_{max} (Dw_{corr}) as in figure 7 and plotted as normalized fluxes (see Appendix 3 for derivation of equations). The red lower curve is equivalent to point A in figure 6. The green and blue lines represent points B'' and C'' in figure 7 using flux averaged recycling factor (f_{avg}) and C_{max} values, representing vascular plants and angiosperm curves respectively.

1997; Landeweert and others, 2001; Lucas, 2001). Although plant roots tend to stop at the water table, they can draw substantial proportions of their water from below this interface without substantially penetrating it (Fan, 2015). Indeed, stable isotopic studies and studies of modern plants show that in many cases, trees tap deep-water sources that should be well below the weathering front (upper few meters of soil) (Stone and Kalisz, 1991; Ehleringer and Dawson, 1992; Jongmans and others, 1997; Kleidon and Heimann, 2000; Landeweert and others, 2001; Lucas, 2001). Thus, about a quarter of the modern global transpiration stream (Evaristo and McDonnell, 2017) is likely to come from below the zone of maximal weathering. The first vascular land plants of the Silurian and Early Devonian would have been exclusively shallow rooting, but the trees of the later Devonian and Carboniferous had deeper roots that would have been able to access the water table in many environments, with water table interactions directly recorded in some rooting fossils (Algeo and others, 2001; Pfefferkorn and Wang, 2009; Boyce and others, 2017).

Given these caveats, we can place some quantitative constraints on the role that plants play in increasing weathering fluxes through time (figs. 7 and 8). For the following estimates, we use our end-members for a no-transpiration world (minimally

vegetated with no deep-rooted vegetation), vascular plant world, and angiosperm world, global average Dw values (0.03 m/yr) from modern constraints (Maher and Chamberlain, 2014), and also include both a precipitation – soil CO_2 – C_{max} relationship and the introduction of a recycling term into the weathering equations. We conclude that moving water vapor inland due to transpiration increases solute concentrations by a factor of 2.39 for vascular plants and by a factor of 2.55 for angiosperms (table 3). This effect was noted by Berner (1992) and Drever (1994) based on climate model results by Shukla and Mintz (1982), but is not modeled explicitly in GEOCARB-SULF (although there is a function incorporated into GEOCARBSULF between increased runoff and increased CO_2 levels; see Berner and Kothavala, 2001; Royer and others, 2014) or more specific process-based models of plant-enhanced weathering (for example, Banwart and others, 2009; Taylor and others, 2009, 2011, 2012; Quirk and others, 2012; Beerling and others, 2012; Thorley and others, 2015). Climate models comparing vegetated versus desert worlds have shown that plant transpiration can double precipitation over land (Kleidon and others, 2000).

Using climate models, Lee and Boyce (2010) (see also Boyce and Lee, 2010, 2011, 2017) have shown that angiosperms—which have a greater transpirative capacity than other vascular-plants—cause an increase in precipitation over continents, although changes in the spatial pattern of precipitation are complex. Moreover, vegetation can increase precipitation over landmasses independent of transpiration via albedo effects (see desert world vs. no-transpiration world maps in Boyce and Lee, 2017). Thus, one would expect that both the advent of pigmented microbial soil communities, followed by the evolution of vascular plants and of angiosperms, played a significant role in increasing weatherability by altering climate. Although this effect is difficult to quantify even with climate models, any long-term carbon cycle model (for example models by, Berner and Kothavala, 2001; Bergman and others, 2004; Berner, 2006; Zeebe, 2012; Mills and others, 2014) must account for this effect.

Increases in precipitation over land due to increases in transpiration must have occurred at least twice in Earth's history: once at the advent of vascular plants, particularly deep-rooted trees in the later Devonian and Carboniferous, and again with the evolution of flowering plants with high transpiration capacities in the latest Cretaceous and early Cenozoic. Transpirative effects on weathering were not likely to be important before this time; for example, during the evolution of the first land plants in the Ordovician through early Devonian, bryophyte-grade and simple shallow-rooting vascular land plants had limited capacity to remobilize soil water in any significant manner (Boyce and Lee, 2017).

Finally, we conclude that angiosperms increased solute concentrations by up to 7 to 55 percent over other vascular plants (point B' or B'' to C' or C'' in Figure 7). The range is due to the unconstrained transition and trajectory between two likely end-members, a weathering system that is independent from plant biomass (represented by A'), to the current state (C'') where biomass and soil CO_2 are correlated to precipitation. The first trajectory is that the transition between both scenarios occur early, linked to the appearance of roots, allowing for colonization of well drained soils and a root system that provides decaying biomass directly to the source (in this case B'' over B' and a 7 percent change in solute concentration between B'' and C''). Alternatively, a second trajectory is supported if the modern relationship between soil CO_2 and precipitation is an angiosperm-only trait, providing a higher flux of decaying biomass to the system for a given precipitation and in that case a transition from B' (or more likely an intermediate value between B' and B") to C'' would occur with the associated 55 percent increase in solute concentration. When compared to other vascular and non-vascular plants, angiosperm leaves have shorter life spans, higher nutrient contents and are paired with higher leaf decay rates (Cornwell and others,

2008), though this difference in decomposability is not necessarily observed in wood or root traits (McCormack and others, 2012), and does not increase soil nitrogen availability (Mueller and others, 2012), leaving it hard to constrain whether the well supported differences in leaf traits play a large role in determining past soil CO_2.

Nevertheless, our results are similar in range and magnitude compared to the output of GEOCARBSULF (Berner, 2006; see also Berner and Kothavala, 2001), where an increase of about 12.5 percent in weathering rates are observed with the transition to angiosperm dominance. This increase due to angiosperm dominance of ecosystems is unlikely to explain the long-term decrease in Cenozoic pCO_2. Though Caves and others (2016a) demonstrated that the strength of the silicate weathering feedback increased during the mid to late Cenozoic, angiosperm ecosystems were well-established by the latest Paleocene, indicating that the reason for long-term declining Cenozoic pCO_2 cannot be attributed to our estimated increase in weathering rates due to the rise of angiosperms. Given that the angiosperm proliferation was in the Late Cretaceous and early Cenozoic and they were already overwhelmingly dominant by the latest Paleogene, another explanation would be needed for further increases in the Neogene. The Neogene spread of grasslands, and associated potential albedo changes—a topic not modeled here—would be an obvious plant-related candidate (Freeman and Colarusso, 2001; Fox and Koch, 2004; Feakins and others, 2005; Edwards and others, 2010; Strömberg, 2011; Chamberlain and others, 2014), though other non-biological factors such as tectonics (for example, Misra and Froelich, 2012; Caves and others, 2016a) are possible.

Though plant evolution has caused a long-term, unidirectional change in the global weathering regime, superimposed on this biological effect are transient climatic (less than 10 Myr) disturbances, such as weathering-erosion perturbations hypothesized for the end-Permian and end-Cretaceous extinction events (see for example McElwain and Punyasena, 2007; Sheldon and others, 2014). Furthermore, the effects described here related to land plant evolution may be overprinted by the longer-term changes in the composition of subaerial continental crust, changes in exposed lithologies, and tectonically induced mountain building, which also influences changes in soil depth and weathering zone thickness (for example, Ronov and others, 1980; Bluth and Kump, 1991; Gibbs and others, 1999; Berner, 2006; Li and Elderfield, 2013).

Taken together, we suggest that weathering concentrations increased due to the rise of plants from a minimally vegetated world to the modern by more than 2-fold (point A to B'' or C'' in fig. 7) due to the combined effects of increases in movement of water vapor by transpiration, in soil CO_2 concentrations, and in thickness of the weathering horizon. This result implies a similar but slightly weaker weathering sensitivity, than the average 4-fold increased used in GEOCARBSULF (Berner, 2006; see also Berner and Kothavala, 2001; Royer and others, 2014; table 3).

Climate Implications

Much of the above discussion focused on the mechanisms—including higher soil pCO_2 and downwind water vapor recycling—by which plant evolution has altered silicate weathering. These mechanisms would have altered the effectiveness of silicate weathering in modulating climate. Here, we discuss how these mechanisms—coupled with the concept of a silicate weathering feedback—likely led to long-term, dramatic changes for the Earth surface.

Though a number of different formulations for the silicate weathering feedback have been proposed (Walker and others, 1981; Berner and others, 1983; Volk, 1987, 1989; Berner and Canfield, 1989; Berner and Kothavala, 2001; Bergman and others, 2004; Berner, 2006; Uchikawa and Zeebe, 2008; Caves and others, 2016a), central to all of these formulations is the idea that the silicate weathering flux is sensitive to climate. In these cases, climate usually refers to temperature, runoff, or pCO_2, such that higher temperatures, greater runoff, or higher pCO_2 results in a greater silicate weathering flux. Here, we

have utilized the formulation of Maher and Chamberlain (2014) (eqs. 5 and 7), which directly links the concentration of silicate-derived solutes to climate through runoff.

The silicate weathering flux is calculated using eq. 1 (reproduced below):

$$F_{sil} = q \times C \tag{1}$$

where C is calculated using eq. 7 (reproduced below):

$$C = C_{max} \frac{f\tau Dw/q}{1 + f\tau Dw/q}, \tag{7}$$

where we have proposed that $f = 1$ prior to plant evolution. The coupling between F_{sil} and climate (q) (that is, strength of the weathering feedback) is modified by the values of C_{max}, f (recycling factor), and Dw. In figure 8, we plot a normalized silicate weathering feedback curve, as represented by F_{sil} as a function of q, prior to plant evolution (lowest red line). In this figure, the silicate weathering feedback is normalized to the value of q required to produce a normalized F_{sil} value of 1 (F_{sil0}). Because F_{sil} must balance the volcanic and metamorphic inputs of carbon on geologic timescales (> 1 Ma), the y-axis is equivalent to the normalized flux of volcanic and metamorphic carbon.

The evolution of vascular plants in the late Devonian increased C_{max} and f; as a consequence, F_{sil} must have increased and then subsequently decreased to match the volcanic and metamorphic flux. Increased F_{sil} would remove CO_2 from the atmosphere, resulting in declining pCO_2 and hence cooling, which would result in lower q. Though the volcanic/solid Earth inputs of carbon may have changed through time (McKenzie and others, 2016), there is no evidence that this flux changed as a consequence of plant evolution. Thus, across the late Devonian, we assume the volcanic and metamorphic inputs remained constant and, thus, F_{sil} must eventually decline following the spread of vascular plants. This decline in F_{sil} is accomplished because q decreases in response to cooling even as C_{max} and f remain higher than prior to the spread of vascular plants. Consequently, the silicate weathering feedback would be characterized by the middle green line in figure 8, which has a higher slope than the pre-vascular plant silicate weathering feedback. Moreover, following the spread of vascular plants, any carbon cycle perturbation would result in a larger increase in F_{sil} than prior to the evolution of plants, thus dampening the climatic impact of such a perturbation. In this sense, the strength of the silicate weathering feedback increases as plants evolve. A similar increase in the strength of the silicate weathering feedback would occur when the evolution of angiosperms further increased C_{max} and f (highest blue line in fig. 8). Thus, the evolution of plants resulted in a long-term decline in the steady-state atmospheric pCO_2, accompanied by decreases in surface temperatures and in runoff—a result also found by others who have modeled the impacts of plant evolution on climate (Berner, 2006; Le Hir and others, 2011).

A major assumption in this analysis is that both C_{max} and f remain largely unchanged even as atmospheric pCO_2 decreased. In reality, C_{max} is influenced by soil pCO_2, which is at least partially influenced by atmospheric pCO_2 (Cerling, 1984). Thus, although soil respiration will be a larger influence after vascular plant evolution (Berner, 1992), C_{max} is still likely to co-vary positively with atmospheric pCO_2. Changes in f are harder to evaluate and ultimately would require a more detailed consideration of the plant biology and of soil depth changes that might have their own complex feedbacks (for example, Sellers and others, 1996; Betts and others, 1997; Swann and others, 2016). For instance, the fraction of precipitation that is partitioned to transpiration would be expected to increase with lower atmospheric pCO_2, as more gas exchange would be required to acquire a given amount of carbon (for example, Ainsworth and Rogers, 2007; Dalling and others, 2016). Conversely, widespread

observations of "greening" (for example, greater leaf-area; see also Skinner and others, 2017) with higher $p\mathrm{CO}_2$—both in the modern (Zhu and others, 2016) and in the geologic past (Caves and others, 2016b)—suggest that global transpiration fluxes may scale with increasing atmospheric $p\mathrm{CO}_2$. Quantifying these additional feedbacks on weathering is beyond the scope of the current study, though they represent unanswered, critical Earth system questions. We note, however, that the modeled changes in C_{max} and f due to plant evolution are likely greater than those induced by feedbacks with changes to long-term atmospheric $p\mathrm{CO}_2$.

The evolution of plants would have thus wrought major changes to the Earth system simply through its impact on silicate weathering. In short, the evolution of plants may have dramatically cooled the climate and reduced runoff normalized to precipitation. At this point, the consequent impacts remain speculative, but likely range from affecting how rivers transported sediment to atmospheric circulation changes (for example, Davies and Gibling, 2003, 2010, 2010; Boyce and Lee, 2010, 2011). Additional quantitative constraints on the impact of plant evolution on silicate weathering, as well as accounting for a richer variety of processes than our simple model permits, will yield further insights into the evolution of our planet's carbon cycle.

CONCLUSION

In this contribution, we used modern empirical and modeling constraints on atmospheric vapor-transport over continents and terrestrial weathering fluxes. We found that the emergence of widespread transpiration and downstream vapor recycling, and subsequent increases in soil $p\mathrm{CO}_2$, would have more than doubled weathering concentrations when deep-rooted vascular plants (Devonian-Carboniferous) fully replaced a minimally vegetated (pre-Devonian) world (fig. 6; table 3). Further, we found that the domination of ecosystems by angiosperms (late Cretaceous and Cenozoic) would have further increased weathering concentrations by an additional 7 to 55 percent. Through this work, we show that incorporating inland vapor recycling—a factor that is not currently incorporated into existing 1-D carbon cycle models—results in a significant change in weathering solute concentrations. This inland vapor recycling increases weathering solute concentrations due to: *(1)* increased total precipitation, which increases soil $p\mathrm{CO}_2$ and hence theoretical maximum aqueous solute concentrations, and *(2)* decreased total runoff that drive the weathering system closer to chemostatic concentrations. This inland vapor recycling would have also increased the likelihood that precipitation reaches inland, cratonic mountain ranges. Partitioning of the vapor recycling effects and feedbacks on weathering thermodynamics indicate that 55 percent of the increase in weathering solute concentrations from a minimally vegetated world to an angiosperm-dominated world is attributed to the thermodynamic effects of increased soil $p\mathrm{CO}_2$, which decreases soil pH and increases equilibrium solute concentrations. While the absolute values of the modeling results carried out in this contribution certainly varied over the Phanerozoic due to long-term changes in erosive regime, volcanic degassing rates, super continent formation, and changes in the solar constant, the trends observed within this modeling framework are indicative of the directionality of change.

Our model results place previously hypothesized effects of plant evolution on the Earth system on a more mechanistic footing. We show that deep-rooted plants can act to modulate weathering fluxes through controlling the hydrologic cycle. To maintain carbon mass balance in vegetated worlds, the higher weatherability of the continental surface must be balanced by a globally averaged lower runoff value. Further, steady-state atmospheric $p\mathrm{CO}_2$ is lower for a more weatherable planet, matching model results following the rise of land plants (for example, Berner, 2006; Le Hir and others, 2011). Finally, the primary implication of this work is that the strength of the silicate weathering feedback increased as plants colonized the continents, in line with observa-

tions that carbon isotope excursions decrease in magnitude over the Phanerozoic (Bachan and others, 2017). Previous models of the impact of plant evolution on biogeochemical cycles have overlooked the importance of inland vapor recycling in setting the strength of this feedback. Thus, we propose that the largest increase in the silicate weathering feedback sensitivity was caused by the deep rooting vascular plants in the late Devonian and Carboniferous, with a smaller feedback sensitivity increase occurring during the expansion of angiosperms in the Cretaceous and Cenozoic.

APPENDIX 1: MODEL 1 DERIVATION

DERIVATION

The mass balance equations.—In the following we derive an advection-diffusion-reaction model simulating the transport of water vapor across a 1-dimensional continental domain. The advection term accounts for directional transport (prevailing winds), diffusion simulates turbulent mixing, and reaction terms account for moisture that is lost to precipitation and returned to the air mass via evapotranspiration. Within a domain of a given length we consider a control volume with dimensions of dx (width) by A (cross-sectional area). The mass balance for the control volume can be expressed as: the time rate of change of mass (TROCM) equals mass-rate-in (MRI) minus mass-rate-out (MRO) plus sources or sinks (S). Or:

$$TROCM = MRI - MRO + S/S$$

where the time (t)-rate of change of water vapor (w) in a grid cell is the volume of the cell times its vapor content:

$$TROCM = \frac{\partial w A dx}{\partial t}$$

and the total water vapor flux per unit time into the control volume (MRI) is the sum of the advective (Q_a) and diffusive fluxes (Q_d):

$$MRI = Q_d + Q_a$$

Each flux is the product of the area-normalized flux and the cross-sectional area:

$$MRI = q_d A + q_a A$$

The inputs (at point x) are known but the outputs (at point x + dx) have to be estimated. We do so by expressing them as a first order Taylor series expansion of the input fluxes in the x direction.

$$MRO = Q_d + \frac{\partial Q_d}{\partial x} dx + Q_a + \frac{\partial Q_a}{\partial x} dx$$

$$MRO = q_d A + \frac{\partial q_d A}{\partial x} dx + q_a A + \frac{\partial q_a A}{\partial x} dx$$

Finally, the reaction terms (S/S), precipitation (P), evaporation (E), and transpiration (T), similarly are considered to scale with the volume of the control volume:

$$S/S = -PAdx + ETAdx + TAdx$$

Putting these equations together and canceling terms:

$$\frac{\partial wAdx}{\partial t} = \frac{\partial q_dA}{\partial x}dx + \frac{\partial q_aA}{\partial x}dx - PAdx + ETAdx$$

Assuming that A and dx are constant across x we can divide through by Adx:

$$\frac{\partial w}{dt} = -\frac{\partial q_d}{dx} - \frac{\partial q_a}{dx} - P + ET = -\frac{\partial}{dx}(q_d + q_a) - P + ET$$

Where the diffusional flux is proportional to the water vapor gradient:

$$q_d = -D\frac{\partial w}{\partial x}$$

And the advective input flux is the transport velocity (u) times the water vapor content:

$$q_a = uw$$

Substituting the flux relationships for q_a and q_d, and assuming that D and w are independent of x (allowing us to move them out of the differential and rearrange) we get a 2nd-order ODE:

$$\frac{\partial w}{\partial t} = D\frac{\partial^2 w}{\partial x^2} - u\frac{\partial w}{\partial x} - P + ET$$

Finally, we solve the system in steady state, so the time derivative is set to zero:

$$0 = D\frac{\partial^2 w}{\partial x^2} - u\frac{\partial w}{\partial x} - P + ET$$

Boundary conditions.—A 2nd-order ODE requires two boundary conditions, one on each side. We assume that the source of moisture is always on the left side of the domain (west side of the continent) while the right side represents the interior or edge of the continent. Each boundary (left or right) can be defined by one of three types of conditions, making a total of 9 different boundary condition combinations. Not all combinations are physically reasonable.

First, we consider a constant flux condition on the left. In this case both the advective and diffusive fluxes sum up to a constant prescribed value so that there is constant net transport of material across the edge of the domain. On the right, all three boundary conditions make physical sense in combination with a constant flux condition on the left.

TABLE A1

Possible combinations of constant flux, constant gradient, and constant gradient boundary conditions on the left and right sides. 'x' defines physically reasonable boundary conditions.

		Left side		
		Constant Flux	Constant Concentration	Constant Gradient
	Constant Flux	x (Figure A5)		
Right Side	Constant Concentration	x	x	
	Constant Gradient	x (Main text; Figure 5)	x	

     a. A constant flux condition on the right with a value of zero means that no moisture crosses the far edge of the domain. This combination of boundary conditions allows for testing of the accuracy of the code, since what comes in must come out. A value other than zero allows a prescribed amount of moisture to leave the domain. This boundary condition combination is shown in Figure A5.

     b. A constant gradient condition on the right with a value of zero enforces a zero gradient condition across the edge of the domain, which effectively means zero diffusive flux. This condition corresponds to the scenario that a balance had been reached between precipitation, evaporation, and transpiration such that no additional gradient in water vapor content remains. Advection then sweeps the remaining moisture off the edge of the domain (that is, the continental mass).

     c. Constant concentration condition with a zero value on the right enforces the condition of zero water vapor on the boundary and thus no advection off the edge.

2. Second, a constant concentration condition on the left with a positive value implies that our domain is connected to a much larger volume of air, so that upon removal of moisture the vapor content of the larger domain remains unchanged. This condition makes physical sense with a constant concentration or a constant gradient condition on the right. A constant flux condition only makes sense if diffusion is more dominant than advection (otherwise it leads to piling up of water vapor on the right side of the domain).

3. Lastly, a constant gradient condition on the left makes little physical sense.

<center>NUMERICAL SOLUTION</center>

<center>*Discretization*</center>

The advection-diffusion-reaction equation can be written as:

$$\frac{\partial w}{\partial t} = -\frac{\partial}{\partial x}\left(-D\frac{\partial w}{\partial x} + uw\right) - P + ET$$

We can integrate over a single cell spanning $x_{i-1/2}$ to $x_{i+1/2}$ and obtain the mass balance for it:

$$\bar{w}_1 = -\int_{x_{i-1/2}}^{x_{i+1/2}} \frac{\partial}{\partial x}\left(-D\frac{\partial w}{\partial x} + uw\right)dx + \bar{s}_1$$

$$\bar{w}_1 = -\left(-D\frac{\partial w}{\partial x} + uw\right)\Big|_{x_{i-1/2}}^{x_{i+1/2}} + \bar{s}_1$$

Where the spatial integral over the time derivative, $\int_{x_{i-1/2}}^{x_{i+1/2}} \frac{\partial w}{\partial x}dx$, on the left side is denoted by $\bar{w}_1$, and the integral over the sources and sinks for the cell, $\int_{x_{i-1/2}}^{x_{i+1/2}}(-P + ET)dx$, by $\bar{s}_1$.

The expression simply states that the change in a mass of material in a cell is the difference between the sum of advective and diffusive fluxes coming in on the left minus those leaving the cell on the right:

$$\bar{w}_1 = \frac{1}{\Delta x}\left(-D\frac{\partial w}{\partial x} + uw\right)_{i-1/2} - \frac{1}{\Delta x}\left(-D\frac{\partial w}{\partial x} + uw\right)_{i+1/2} + \bar{s}_1$$

For the advective flux, we estimate the value at the boundary by linear interpolation:

$$uw_{i-1/2} = u\frac{w_{i-1} + w_i}{2}$$

For diffusion, we estimate the derivative by a first order difference:

$$-D\frac{dw}{dx}\Big|_{i-1/2} = -D\frac{w_i - w_{i-1}}{\Delta x}$$

Substituting the quantities yields:

$$\bar{w}_l = \left(\frac{D}{\Delta x^2} + \frac{u}{2\Delta x}\right)w_{i-1} - \frac{2D}{\Delta x^2}w_i + \left(\frac{D}{\Delta x^2} + \frac{u}{2\Delta x}\right)w_{i+1} + \bar{S}_l$$

Equivalently one can use first-ordered centered in space discretization for both the first and second order terms:

$$\frac{\partial^2 w}{\partial x^2} \approx \frac{w_{i-1} - 2w_i + w_{i+1}}{\Delta x^2}$$

$$\frac{\partial w}{\partial x} \approx \frac{w_{i+1} - w_{i-1}}{2\Delta x}$$

And replace them in the equation steady state equation, which yields the same result:

$$\left(\frac{D}{\Delta x^2} + \frac{u}{2\Delta x}\right) w_{i-1} - \frac{2D}{\Delta x^2} w_i + \left(\frac{D}{\Delta x^2} - \frac{u}{2\Delta x}\right) w_{i+1} - P_i + ET_i = 0$$

To simplify we denote the constant coefficients with the letter C:

$$C_{i-1} w_{i-1} + C_i w_i + C_{i+1} w_{i+1} - P_i + ET_i = 0$$

Where

$$C_{i-1} = \left(\frac{D}{\Delta x^2} + \frac{u}{2\Delta x}\right); \ C_i = \frac{2D}{\Delta x^2}; \ C_{i+1} = \left(\frac{D}{\Delta x^2} - \frac{u}{2\Delta x}\right)$$

Boundary Condition Implementation

Constant flux conditions.—In the finite volume method, constant flux boundary conditions that define a total flux are naturally resolved, and require no discretization. Specifically, the condition is that the total flux on the right side of the domain is given by:

$$\left(uw - D\frac{dw}{dx}\right)_{1/2} = w_{in}$$

So within the context of the finite volume balance:

$$\bar{w}_1 = \frac{1}{\Delta x}\left(-D\frac{\partial w}{\partial x} + uw\right)_{1/2} - \frac{1}{\Delta x}\left(-D\frac{\partial w}{\partial x} + uw\right)_{3/2} + \bar{s}_1$$

$$\bar{w}_1 = \frac{w_{in}}{\Delta x} - \frac{1}{\Delta x}\left(-D\frac{\partial w}{\partial x} + uw\right)_{3/2} + \bar{s}_1$$

Using the approximations for the advective and diffusive fluxes:

$$\bar{w}_1 = \frac{w_{in}}{\Delta x} - \frac{1}{\Delta x}\left(-D\frac{w_2 - w_1}{\Delta x} + u\frac{w_2 + w_1}{2}\right) + \bar{s}_1$$

$$\bar{w}_1 = \frac{w_{in}}{\Delta x} - C_{i-1} w_1 + C_{i+1} w_2 + \bar{s}_1$$

Similarly, on the right boundary of the domain at location 'n':

$$\bar{w}_n = \frac{1}{\Delta x}\left(-D\frac{w_n - w_{n-1}}{\Delta x} + u\frac{w_n + w_{n-1}}{2}\right) - \frac{w_{out}}{\Delta x} + \bar{s}_n$$

$$\bar{w}_n = C_{i-1} w_{n-1} + C_{i+1} w_n - \frac{w_{out}}{\Delta x} + \bar{s}_n$$

Constant concentration conditions.—The implementation of constant concentration condition is simple. In this case, the value of w in the first (or last) cell is known. So:

$$1 w_1 + 0 w_2 + 0 w_3 - (P_i + ET_i) * 0 = w_{in}$$

Thus, we set the corresponding coefficients such that all terms other than w_1 vanish and add - w_{in} in our boundary conditions vector.

Constant gradient conditions.—In the case of constant gradient boundary conditions the diffusional flux across the edge of the domain is known:

$$-D\,\frac{\partial w}{\partial x} \;=\; w_{out}$$

Discretizing for the right edge:

$$-D\,\frac{w_{n+1} \;-\; w_n}{\Delta x} \;=\; w_{out}$$

$$w_{n+1} \;=\; w_n \;-\; \frac{\Delta x}{D}\,w_{out}$$

Substituting coefficients:

$$C_{i-1}w_{n-1} \;+\; C_i w_n \;+\; C_{i+1}\!\left(w_n \;-\; \frac{\Delta x}{D}w_{out} \right) \;-\; P_i \;+\; ET_i \;=\; 0$$

$$C_{i-1}w_{n-1} \;+\; (C_i \;+\; C_{i+1})\,w_n \;-\; C_{i+1}\frac{\Delta x}{D}w_{out} \;-\; P_i \;+\; ET_i \;=\; 0$$

Now discretizing for the left side:

$$-D\,\frac{w_1 \;-\; w_0}{\Delta x} \;=\; w_{out}$$

$$w_0 \;=\; w_{1+}\frac{\Delta x}{D}w_{out}$$

Which using the coefficients goes to:

$$C_{i-1}\frac{\Delta x}{D}w_{out} \;+\; (C_i \;+\; C_{i-1})\,w_1 \;+\; C_{i+1}w_2 \;-\; P_i \;+\; ET_i \;=\; 0$$

MATRIX SETUP and INCORPORATION OF BUDYKO

As an example using the two constant flux boundary conditions, we discretize our equations (in this example with 6 cells), which gives the following matrix:

$$
\begin{bmatrix}
-C_{i-1} & C_{i+1} & 0 & 0 & 0 & 0 \\
C_{i-1} & C_i & C_{i+1} & 0 & 0 & 0 \\
0 & C_{i-1} & C_i & C_{i+1} & 0 & 0 \\
0 & 0 & C_{i-1} & C_i & C_{i+1} & 0 \\
0 & 0 & 0 & C_{i-1} & C_i & C_{i+1} \\
0 & 0 & 0 & 0 & C_{i-1} & -C_{i+1}
\end{bmatrix}
\begin{bmatrix}
w_1 \\ w_2 \\ w_3 \\ w_4 \\ w_5 \\ w_6
\end{bmatrix}
+
\begin{bmatrix}
-P_1 + ET_1 \\
-P_2 + ET_2 \\
-P_3 + ET_3 \\
-P_4 + ET_4 \\
-P_5 + ET_5 \\
-P_6 + ET_6
\end{bmatrix}
+
\begin{bmatrix}
w_{in}/\Delta x \\ 0 \\ 0 \\ 0 \\ 0 \\ w_{out}/\Delta x
\end{bmatrix}
= 0
$$

We use the Budyko relationship to define how precipitation relates to the sum of evaporation and transpiration. Evaporation and transpiration are not partitioned explicitly in this modeling framework. We define precipitation to be a linear function of the water vapor content:

$$P \;=\; k_p w$$

And define the evapotranspiration (E+T=ET) as a function of both precipitation and potential evapotranspiration (E_p) following the formulation used by Greve and others (2015):

$$ET \;=\; P \;+\; E_p \;-\; (P^\omega \;+\; E_p{}^\omega)^{1/\omega}$$

When $\omega=1$, ET=0. As the source (ET) and sink (P) terms are non-linear functions of vapor content (w), we use a root-finding procedure to simultaneously solve for the unknowns in the above matrix (w_i), rather than a matrix inversion method. We implement the model using the multiroot function in the R package 'rootSolve' (Soetaert, 2016), which uses a numerical Newton-Raphson method to find the roots of the above equations.

TABLE A2

APPENDIX 2: COMPILATION OF MODERN TRANSPIRATION MODIFICATION STUDIES

Treatment sites from Bosch and Hewlett (1982) (see their Table 1), and Zhang and others (1999) used to test the effect of reduced canopy transpiration on Budyko relationships (fig. 2B) with 100% treatment (full clear-cutting), all P, q and E_p units are mm/yr. E_p values were calculated as estimated via spatial interpolation from Trabucco and Zomer (2009)

Watershed	Lat	Lon	% Angio	Control		Treatment		E_p
				P	q	P	q	
Alum Creek, AR, USA	34.79	-93.02	0	1333	153	1333	379	1297
Beaver Creek, UT, USA	34.50	-111.50	0	457	20	457	20	1223
Coweeta, NC, USA	35.06	-83.43	100	1900	889	1900	1251	1397
Coweeta, NC, USA	35.06	-83.43	100	1725	739	1725	889	1397
Coyote Creek, OR, USA	43.90	-123.18	0	1230	627	1230	987	1022
Burns (Entiat), WA, USA	47.95	120.47	0	597	155	597	229	623
Fox (Entiat), WA, USA	47.95	120.47	0	597	175	597	287	623
McCree (Entiat), WA, USA	47.95	120.47	0	579	112	579	203	623
Grant Forest, GA, USA	33.38	-83.47	100	1219	467	1219	721	1397
H.J. Andrews, OR, USA	44.21	-122.26	0	2388	1376	2388	1838	1035
Hubbard Brook, NH, USA	43.95	71.72	100	1219	710	1219	1053	829
Kamabuchi (2), Japan	38.93	140.25	60	2641	2075	2641	2181	892
Karuah (Corkwood), Australia	32.20	151.71	100	1637	456	1639	503	1225
Karuah (Jackwood), Australia	32.20	151.71	100	1429	307	1368	313	1225
Karuah, (Kokata), Australia	32.20	151.71	100	1429	307	1562	518	1225
Kimakia, Kenya	-0.90	36.80	100	2014	568	2014	1025	1520
Maimai, New Zealand	-42.08	171.80	~50	2600	1500	2600	2150	811
Natural Drainages AZ, USA	36.05	-114.86	100	452	34	452	34	1471
Natural Drainages, AZ, USA	36.05	-114.86	100	452	43	452	56	1471
Placer County, CA, USA	38.98	121.23	100	635	145	635	256	1352
Wagon Wheel Gap, CO, USA	37.77	-106.83	0	536	157	536	191	979

APPENDIX 3: DERIVATION OF NORMALIZED WEATHERING EQUATIONS

To show the sensitivity of the weathering equations, we normalize the equations from Maher and Chamberlain (2014) following von Blanckenburg and others (2015) (their Figure 3). The solute production model predicts concentration (C) as a function of runoff, with assumed values for Damköhler coefficient and maximum concentration (C_{max}), with a scaling factor ($\tau = e^2$) (equation 4 from the main text):

$$C = C_{max} \frac{\tau Dw/q}{1 + \tau Dw/q}$$

Area normalized weathering flux ($Fsil$) is given by:

$$Fsil = qC_{max} \frac{\tau Dw/q}{1 + \tau Dw/q}$$

Normalizing this equation by a baseline weathering flux ($Fsil_0$) at a given baseline runoff value (q_0) gives:

$$\frac{Fsil}{Fsil_0} = \frac{1 + \tau Dw/q_0}{1 + \tau Dw/q}$$

Note that this assumes no change in C_{max}, which cancels. If C_{max} does not cancel the normalized equation is:

$$\frac{Fsil}{Fsil_0} = \left(\frac{C_{max}}{C_{max_0}} \right) \left(\frac{1 + \tau Dw/q_0}{1 + \tau Dw/q} \right)$$

In figure 8, we use the above relationships to plot normalized fluxes for scenarios A, B'' and C'' of figure 7. For points B'' and C'' we also included the recycling term (f) as a multiplier before Dw (see text for details).
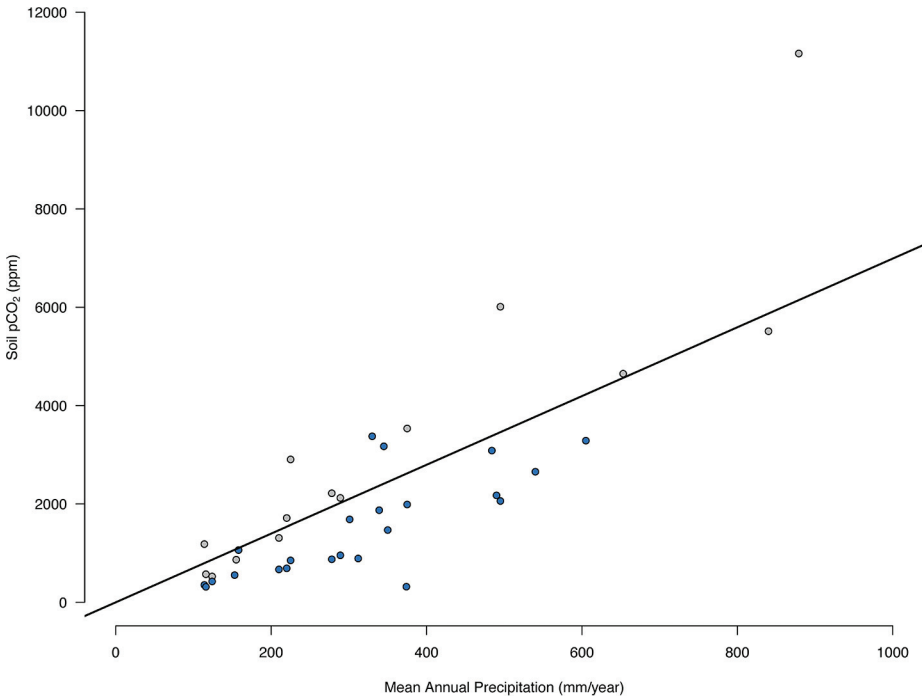
APPENDIX 4: SOIL CO_2–PRECIPITATION RELATIONSHIP

Fig. A4. Relationship between soil pCO_2 and P, calculated as a linear fit to the datasets from Cotton and Sheldon (2012) (blue points) and Cotton and others (2013) (gray points).

APPENDIX 5: ALTERNATE BOUNDARY CONDITION EXAMPLE

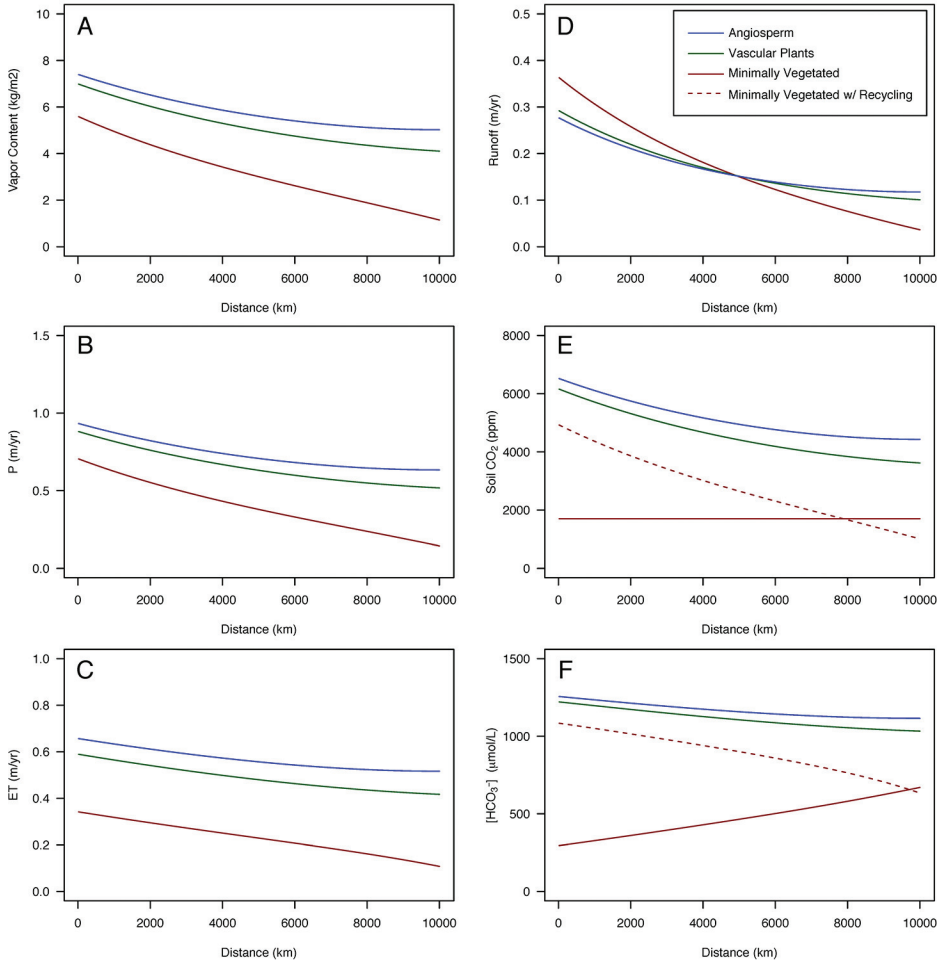## Constant Flux to Constant Flux Boundary Conditions

Fig. A5. Water and solute fluxes simulated using constant flux to constant flux boundary conditions (see text for explanation). Simulations are shown for ω values representing the simulations from Boyce and Lee (2010) and modern observations as in figure 2. Model 1: (A) Total water vapor content, (B) precipitation, (C) evapotranspiration, and (D) runoff. The flux out on the right (eastern) boundary condition was set to 40% of the incoming water vapor, comparable to the Angiosperm simulations shown in figure 5. Model 2: (E) soil $p\mathrm{CO_2}$; and (F) solute $[\mathrm{HCO_3^-}]$ calculated including both hydrologic and thermodynamic feedbacks.

APPENDIX 6: SENSITIVITY OF CALCULATIONS
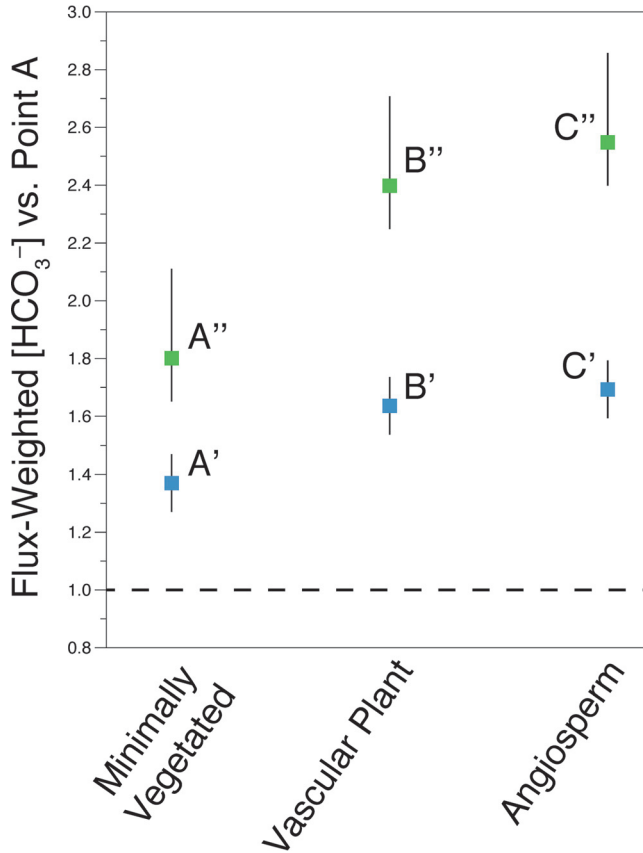
Fig. A6. Sensitivity of normalized [HCO_3^-] calculations for points discussed in the text (A'-C' and A''-C''). The dashed line corresponds to point A. Blue dots show uncertainty (10%) from the Budyko omega parameter propagation of hydrologic effects only (A', B' and C' in fig. 7). Green dots show total uncertainty (+31%/-15%) for propagation of thermodynamic temperature effects and hydrologic effects (A'', B'' and C'' in fig. 7).

REFERENCES

Ainsworth, E. A., and Rogers, A., 2007, The response of photosynthesis and stomatal conductance to rising [CO_2]: Mechanisms and environmental interactions: Plant, Cell and Environment, v. 30, n. 3, p. 258–270, https://doi.org/10.1111/j.1365-3040.2007.01641.x

Algeo, T. J., and Scheckler, S. E., 1998, Terrestrial-marine teleconnections in the Devonian: Links between the evolution of land plants, weathering processes, and marine anoxic events: Philosophical Transactions of the Royal Society B: Biological Sciences, v. 353, n. 1365, p. 113–130, https://doi.org/10.1098/rstb.1998.0195

Algeo, T. J., Berner, R. A., Maynard, J. B., and Scheckler, S. E., 1995, Late Devonian oceanic anoxic events and biotic crises: "Rooted" in the evolution of vascular land plants: GSA Today, v. 5, n. 3, p. 45, 64–66.

Algeo, T. J., Scheckle, S. E., and Maynard, J. B., 2001, Effects of the Middle to Late Devonian spread of vascular land plants on weathering regimes, marine biotas, and global climate, *in* Gensel, P. G., and Edwards, D., editors, Plants invade the land: Evolutionary and environmental perspectives: New York, Columbia University Press, p, 213–236.

Alkama, R., Kageyama, M., and Ramstein, G., 2012, A sensitivity study to global desertification in cold and warm climates: Results from the IPSL OAGCM model: Climate Dynamics, v. 38, n. 7–8, p. 1629–1647, https://doi.org/10.1007/s00382-011-1101-6

Andrews, J. A., and Schlesinger, W. H., 2001, Soil CO_2 dynamics, acidification and chemical weathering in a

temperate forest with experimental CO_2 enrichment: Global Biogeochemical Cycles, v. 15, n. 1, p. 149–162, https://doi.org/10.1029/2000GB001278

Arora, V. K., 2002, The use of the aridity index to assess climate change effect on annual runoff: Journal of Hydrology, v. 265, n. 1–4, p. 164–177, https://doi.org/10.1016/S0022-1694(02)00101-4

Arthur, M. A., and Fahey, T. J., 1993, Controls on soil solution chemistry in a subalpine forest in north-central Colorado: Soil Science Society of America Journal, v. 57, n. 4, p. 1123–1130, https://doi.org/10.2136/sssaj1993.03615995005700040040x

Bachan, A., Lau, K. V., Saltzman, M. R., Thomas, E., Kump, L. R., and Payne, J. L., 2017, A model for the decrease in amplitude of carbon isotope excursions across the Phanerozoic: American Journal of Science, v. 317, n. 6, p. 641–676, https://doi.org/10.2475/06.2017.01

Banwart, S. A., Berg, A., and Beerling, D. J., 2009, Process-based modeling of silicate mineral weathering responses to increasing atmospheric CO_2 and climate change: Global Biogeochemical Cycles, v. 23, n. 4, https://doi.org/10.1029/2008GB003243

Barker, W. W., Welch, S. A., and Banfield, J. F., 1997, Biogeochemical weathering of silicate minerals: Reviews in Mineralogy, v. 35, p. 419–428.

Beerling, D. J., Taylor, L. L., Bradshaw, C. D. C., Lunt, D. J., Valdes, P. J., Banwart, S. A., Pagani, M., and Leake, J. R., 2012, Ecosystem CO_2 starvation and terrestrial silicate weathering: Mechanisms and global-scale quantification during the late Miocene: Journal of Ecology, v. 100, n. 1, p. 31–41, https://doi.org/10.1111/j.1365-2745.2011.01905.x

Berner, R., 1987, Models for carbon and sulfur cycles and atmospheric oxygen: Application to Paleozoic geologic history: American Journal of Science, v. 287, n. 3, p. 177–196, https://doi.org/10.2475/ajs.287.3.177

—— 1991, A model for atmospheric CO_2 over Phanerozoic time: American Journal of Science: v. 291, n. 4, p. 339–376, https://doi.org/10.2475/ajs.291.4.339

—— 1992, Weathering, plants, and the long-term carbon cycle: Geochimica et Cosmochimica Acta, v. 56, n. 8, p. 3225–3231, https://doi.org/10.1016/0016-7037(92)90300-8

—— 1994, GEOCARB II: A revised model of atmospheric CO_2 over Phanerozoic time: American Journal of Science, v. 294, n. 1, p. 56–91, https://doi.org/10.2475/ajs.294.1.56

—— 1998, The carbon cycle and CO_2 over Phanerozoic time: The role of land plants: Philosophical Transactions Royal Society of London, Series B, v. 353, p. 75 – 82, https://doi.org/10.1098/rstb.1998.0192

—— 2004, The Phanerozoic carbon cycle: CO_2 and O_2: New York, Oxford University Press, 150 p.

—— 2006, GEOCARBSULF: A combined model for Phanerozoic atmospheric O_2 and CO_2: Geochimica et Cosmochimica Acta, v. 70, n. 23, p. 5653–5664, https://doi.org/10.1016/j.gca.2005.11.032

—— 2008, Addendum to "Inclusion of the Weathering of Volcanic Rocks in the GEOCARBSULF Model" (R. A. Berner, 2006, v. 306, p. 295–302): American Journal of Science, v. 308, n. 1, p. 100–103, https://doi.org/10.2475/01.2008.04

Berner, R. A., and Caldeira, K., 1997, The need for mass balance and feedback in the geochemical carbon cycle: Geology, v. 25, n. 10, p. 955–956, https://doi.org/10.1130/0091-7613(1997)025<0955:TNFMBA>2.3.CO;2

Berner, R. A., and Canfield, D. E., 1989, A new model for atmospheric oxygen over Phanerozoic time: American Journal of Science, v. 289, n. 4, p. 333–361, https://doi.org/10.2475/ajs.289.4.333

Berner, R. A., and Kothavala, Z., 2001, Geocarb III: A Revised Model of Atmospheric CO_2 over Phanerozoic Time: American Journal of Science, v. 301, n. 2, p. 182–204, https://doi.org/10.2475/ajs.301.2.182

Berner, R. A., and Rao, J.-L., 1996, Alkalinity buildup during silicate weathering under a snow cover: Aquatic Geochemistry, v. 2, n. 4, p. 301–312, https://doi.org/10.1007/BF00115974

Berner, R. A., Lasaga, A. C., and Garrels, R. M., 1983, The carbonate-silicate geochemical cycle and its effect on atmospheric carbon dioxide over the past 100 million years: American Journal of Science, v. 283, n. 7, p. 641–683, https://doi.org/10.2475/ajs.283.7.641

Berner, E. K., Berner, R. A., and Moulton, K. L., 2003, Plants and Mineral Weathering: Present and Past: Treatise on Geochemistry, v. 5, p. 169–188, https://doi.org/10.1016/B0-08-043751-6/05175-6

Bergman, N. M., Lenton, T. M., and Watson, A. J., 2004, COPSE: A new model of biogeochemical cycling over Phanerozoic time: American Journal of Science, v. 304, n. 5, p. 397–437, https://doi.org/10.2475/ajs.304.5.397

Bershaw, J., 2018, Controls on Deuterium Excess across Asia: Geosciences, v. 8, n. 7, p. 257, https://doi.org/10.3390/geosciences8070257

Bethke, C., 2007, Geochemical and Biogeochemical Reaction Modeling: Cambridge, England, Cambridge University Press, 564 p.

Betts, R. A., Cox, P. M., Lee, S. E., and Woodward, F. I., 1997, Contrasting physiological and structural vegetation feedbacks in climate change simulations: Nature, v. 387, p. 796–799, https://doi.org/10.1038/42924

Blanc, P., Lassin, A., Piantone, P., Azaroual, M., Jacquemet, N., Fabbri, A., and Gaucher, E. C., 2012, Thermoddem: A geochemical database focused on low temperature water/rock interactions and waste materials: Applied Geochemistry, v. 27, n. 10, p. 2107–2116, https://doi.org/10.1016/j.apgeochem.2012.06.002

Blum, A. and Lasaga, A. C., 1988, Role of surface speciation in the low-temperature dissolution of minerals: Nature, v. 331, p. 431–433, https://doi.org/10.1038/331431a0

Blum, J. D., Klaue, A., Nezat, C. A., Driscoll, C. T., Johnson, C. E., Siccama, T. G., Eagar, C., Fahey, T. J., and Likens, G. E., 2002, Mycorrhizal weathering of apatite as an important calcium source in base-poor forest ecosystems: Nature, v. 417, p. 729–731, https://doi.org/10.1038/nature00793

Bluth, G. J. S., and Kump, L. R., 1991, Phanerozoic paleogeology: American Journal of Science, v. 291, n. 3, p. 284–308, https://doi.org/10.2475/ajs.291.3.284

―――― 1994, Lithologic and climatologic controls of river chemistry: Geochimica et Cosmochimica Acta, v. 58, n. 10, p. 2341–2359, https://doi.org/10.1016/0016-7037(94)90015-9

Bormann, B. T., Wang, D., Snyder, M. C., Bormann, F. H., Benoit, G., and April, R., 1998, Rapid plant induced weathering in an aggrading experimental ecosystem: Biogeochemistry, v. 43, n. 2, p. 129–155, https://doi.org/10.1023/A:1006065620344

Bosch, J. M., and Hewlett, J. D., 1982, A review of catchment experiments to determine the effect of vegetation changes on water yield and evapotranspiration: Journal of Hydrology, v. 55, n. 1–4, p. 3–23, https://doi.org/10.1016/0022-1694(82)90117-2

Boyce, C. K., and Lee, J. E., 2010, An exceptional role for flowering plant physiology in the expansion of tropical forests and biodiversity: Proceedings Royal Society B, Biological Sciences, v. 277, n. 1699, p. 3437–3443, https://doi.org/10.1098/rspb.2010.0485

―――― 2011, Could Land Plant Evolution Have Fed the Marine Revolution?: Paleontological Research, v. 15, n. 2, p. 100–105, https://doi.org/10.2517/1342-8144-15.2.100

―――― 2017, Plant Evolution and Climate over Geological Timescales: Annual Review of Earth and Planetary Sciences, v. 45, p. 61–87, https://doi.org/10.1146/annurev-earth-063016-015629

Boyce, C. K., and Zwieniecki, M. A., 2012, Leaf fossil record suggests limited influence of atmospheric CO_2 on terrestrial productivity prior to angiosperm evolution: Proceedings of the National Academy of Sciences of the United States of America, v. 109, n. 26, p. 10403–10408, https://doi.org/10.1073/pnas.1203769109

Boyce, C. K., Fan, Y., and Zwieniecki, M. A., 2017, Did trees grow up to the light, up to the wind, or down to the water? How modern high productivity colors perception of early plant evolution: The New Phytologist, v. 215, n. 2, p. 552–557, https://doi.org/10.1111/nph.14387

Breecker, D. O., Sharp, Z. D., and McFadden, L. D., 2009, Seasonal bias in the formation and stable isotopic composition of pedogenic carbonate in modern soils from central New Mexico, USA: Geological Society of America Bulletin, v. 121, n. 3–4, p. 630–640, https://doi.org/10.1130/B26413.1

Broecker, W. S., and Sanyal, A., 1998, Does atmospheric CO_2 police the rate of chemical weathering?: Global Biogeochemical Cycles, v. 12, n. 3, p. 403–408, https://doi.org/10.1029/98GB01927

Brook, G. A., Folkoff, M. E., and Box, E. O., 1983, A world model of soil carbon dioxide: Earth Surface Processes and Landforms, v. 8, p. 79–88, https://doi.org/10.1002/esp.3290080108

Brown, A. E., Zhang, L., McMahon, T. A., Western, A. W., and Vertessy, R. A., 2005, A review of paired catchment studies for determining changes in water yield resulting from alterations in vegetation: Journal of Hydrology, v. 310, n. 1–4, p. 28–61, https://doi.org/10.1016/j.jhydrol.2004.12.010

Brubaker, K. L., Entekhabi, D., and Eagleson, P. S., 1993, Estimation of Continental Precipitation Recycling: Journal of Climate, v. 6, p. 1077–1089, https://doi.org/10.1175/1520-0442(1993)006<1077:EOCPR>2.0.CO;2

Budyko, M. I., 1974, Climate and Life: Orlando, Florida, Academic Press, 508 p.

Burnham, R. J., and Johnson, K. R., 2004, South American paleobotany and the origins of neotropical rainforests: Philosophical Transactions Royal Society of London, Series B, v. 359, p. 1595–1610, https://doi.org/10.1098/rstb.2004.1531

Caves, J. K., Winnick, M. J., Graham, S. A., Sjostrom, D. J., Mulch, A., and Chamberlain, C. P., 2015, Role of the westerlies in Central Asia climate over the Cenozoic: Earth and Planetary Science Letters, v. 428, p. 33–43, https://doi.org/10.1016/j.epsl.2015.07.023

Caves, J. K., Jost, A. B., Lau, K. V., and Maher, K., 2016a, Cenozoic carbon cycle imbalances and a variable weathering feedback: Earth and Planetary Science Letters, v. 450, p. 152–163, https://doi.org/10.1016/j.epsl.2016.06.035

Caves, J. K., Moragne, D. Y., Ibarra, D. E., Bayshashov, B. U., Gao, Y., Jones, M. M., Zhamangara, A., Arzhannikova, A. V., Arzhannikov, S. G., and Chamberlain, C. P., 2016b, The Neogene de-greening of Central Asia: Geology, v. 44, n. 11, p. 887–890, https://doi.org/10.1130/G38267.1

Cerling, T. E., 1984, The stable isotopic composition of modern soil carbonate and its relationship to climate: Earth and Planetary Science Letters, v. 71, n. 2, p. 229–240, https://doi.org/10.1016/0012-821X(84)90089-X

Chamberlain, C. P., Winnick, M., Mix, H. T., Chamberlain, S. D., and Maher, K., 2014, The impact of Neogene grassland expansion and aridification on the isotopic composition of continental precipitation: Global Biogeochemical Cycles, v. 28, n. 9, p. 922–1004, https://doi.org/10.1002/2014GB004822

Choudhury, B. J., 1999, Evaluation of an empirical equation for annual evaporation using field observations and results from a biophysical model: Journal of Hydrology, v. 216, n. 1–2, p. 99–110, https://doi.org/10.1016/S0022-1694(98)00293-5

Colbourn, G., Ridgwell, A., and Lenton, T. M., 2015, The time scale of the silicate weathering negative feedback on atmospheric CO_2: Global Biogeochemical Cycles, v. 29, n. 5, p. 583–596, https://doi.org/10.1002/2014GB005054

Coogan, L. A., and Gillis, K. M., 2013, Evidence that low-temperature oceanic hydrothermal systems play an important role in the silicate-carbonate weathering cycle and long-term climate regulation: Geochemistry, Geophysics, Geosystems, v. 14, n. 6, p. 1771–1786, https://doi.org/10.1002/ggge.20113

Cornwell, W. K., Cornelissen, J. H. C., Amatangelo, K., Dorrepaal, E., Eviner, V. T., Godoy, O., Hobbie, S. E., Hoorens, B., Kurokawa, H., Pérez-Harquindeguy, N., Quested, H. M., Santiago, L. S., Wardle, D. A., Wright, I. J., Aerts, R., Allison, S. D., Van Bodegom, P., Brovkin, V., Chattain, A., Callaghan, T. V., Díaz, S., Garnier, E., Gurvich, D. E., Kazakou, E., Klein, J. A., Read, J., Reich, P. B., Soudzilovskaia, N. A., Vaieretti, M. V., and Westoby, M., 2008, Plant species traits are the predominant control on litter decomposition rates within biomes worldwide: Ecology letters, v. 11, n. 10, p. 1065–1071, https://doi.org/10.1111/j.1461-0248.2008.01219.x

Cotton, J. M., and Sheldon, N. D., 2012, New constraints on using paleosols to reconstruct atmospheric

pCO_2: Bulletin of the Geological Society of America, v. 124, n. 9–10, p. 1411–1423, https://doi.org/10.1130/B30607.1

Cotton, J. M., Jeffery, M. L., and Sheldon, N. D., 2013, Climate controls on soil respired CO_2 in the United States: Implications for 21st century chemical weathering rates in temperate and arid ecosystems: Chemical Geology, v. 358, p. 37–45, https://doi.org/10.1016/j.chemgeo.2013.08.048

Crane, P. R., and Lidgard, S., 1989, Angiosperm diversification and paleolatitudinal gradients in Cretaceous floristic diversity: Science, v. 246, n. 4930, p. 675–678, https://doi.org/10.1126/science.246.4930.675

Dalling, J. W., Cernusak, L. A., Winter, K., Aranda, J., Garcia, M., Virgo, A., Alexander, W. C., Baresch, A., Jaramillo, C., and Turner, B. L., 2016, Two tropical conifers show strong growth and water-use efficiency responses to altered CO_2 concentration: Annals of Botany, v. 118, n. 6, p. 1113–1125, https://doi.org/10.1093/aob/mcw162

Davies, S. J., and Gibling, M. R., 2003, Architecture of coastal and alluvial deposits in an extensional basin: The Carboniferous Joggins Formation of eastern Canada: Sedimentology, v. 50, n. 3, p. 415–439, https://doi.org/10.1046/j.1365-3091.2003.00553.x

——— 2010, Cambrian to Devonian evolution of alluvial systems: The sedimentological impact of the earliest land plants: Earth-Science Reviews, v. 98, n. 3–4, p. 171–200, https://doi.org/10.1016/j.earscirev.2009.11.002

Des Marias, D. J., 1990, Microbial mats and the early evolution of life: Trends in Ecology and Evolution, v. 5, n. 5, p. 140–144, https://doi.org/10.1016/0169-5347(90)90219-4

Dessert, C., Dupré, B., Gaillardet, J., François, L. M., and Allègre, C. J., 2003, Basalt weathering laws and the impact of basalt weathering on the global carbon cycle: Chemical Geology, v. 202, n. 3–4, p. 257–273, https://doi.org/10.1016/j.chemgeo.2002.10.001

Dixon, J. L., and von Blanckenburg, F., 2012, Soils as pacemakers and limiters of global silicate weathering: Comptes Rendus Geoscience, v. 344, n. 11–12, p. 597–609, https://doi.org/10.1016/j.crte.2012.10.012

Domeier, M., and Torsvik, T. H., 2014, Plate tectonics in the late Paleozoic: Geoscience Frontiers, v. 5, n. 3, p. 303–350, https://doi.org/10.1016/j.gsf.2014.01.002

Donnadieu, Y., Goddéris, Y., Ramstein, G., Nédélec, A., and Meert, J., 2004, A "snowball Earth" climate triggered by continental break-up through changes in runoff: Nature, v. 428, n. 6980, p. 303–306, https://doi.org/10.1038/nature02408

Donnadieu, Y., Goddéris, Y., Pierrehumbert, R., Dromart, G., Fluteau, F., and Jacob, R., 2006, A GEOCLIM simulation of climatic and biogeochemical consequences of Pangea breakup: Geochemistry, Geophysics, Geosystems, v. 7, n. 11, https://doi.org/10.1029/2006GC001278

Donnadieu, Y., Goddéris, Y., and Bouttes, N., 2009, Exploring the climatic impact of the continental vegetation on the Mezosoic atmospheric CO_2 and climate history: Climate of the Past, v. 5, n. 1, p. 85–96, https://doi.org/10.5194/cp-5-85-2009

Drever, J. I., 1994, The effect of land plants on weathering rates of silicate minerals: Geochimica et Cosmochimica Acta, v. 58, n. 10, p. 2325–2332, https://doi.org/10.1016/0016-7037(94)90013-2

Drever, J. I., and Zobrist, J., 1992, Chemical weathering of silicate rocks as a function of elevation in the southern Swiss Alps: Geochimica et Cosmochimica Acta, v. 56, n. 8, p. 3209–3216, https://doi.org/10.1016/0016-7037(92)90298-W

Edwards, E. J, Osborne, C. P., Stromberg, C. A. E., Smith, S. A., and the C4 Grasses Consortium, 2010, The origins of C_4 grasslands: Integrating evolutionary and ecosystem science: Science, v. 328, n. 5978, p. 587–591, https://doi.org/10.1126/science.1177216

Ehleringer, J. R., and Dawson, T. E., 1992, Water uptake by plants: Perspectives from stable isotope composition: Plant, Cell & Environment, v. 15, n. 9, p. 1073–1082, https://doi.org/10.1111/j.1365-3040.1992.tb01657.x

Evaristo, J., and McDonnell, J.J., 2017, Prevalence and magnitude of groundwater use by vegetation: A global stable isotope meta-analysis: Scientific Reports, v. 7, article number 44110, https://doi.org/10.1038/srep44110

Fan, Y., 2015, Groundwater in the Earth's critical zone: Relevance to large-scale patterns and processes: Water Resources Research, v. 51, n. 5, p. 3052–3069, https://doi.org/10.1002/2015WR017037

Feakins, S. J., deMenocal, P. B., and Eglinton, T. I., 2005, Biomarker records of late Neogene changes in northeast African vegetation: Geology, v. 33, n. 12, p. 977–980, https://doi.org/10.1130/G21814.1

Foster, G. L., Royer, D. L., and Lunt, D. J., 2017, Future climate forcing potentially without precedent in the last 420 million years: Nature Communications, v. 8, p. 14845, https://doi.org/10.1038/ncomms14845

Fox, D. L., and Koch, P. L., 2004, Carbon and oxygen isotopic variability in Neogene paleosol carbonates: Constraints on the evolution of the C_4-grasslands of the Great Plains, USA: Palaeogeography, Palaeoclimatology, Palaeoecology, v. 207, n. 3–4, p. 305–329, https://doi.org/10.1016/j.palaeo.2003.09.030

Fraedrich, K., Kleidon, A., and Lunkeit, F., 1999, A Green Planet versus a Desert World: Estimating the Effect of Vegetation Extremes on the Atmosphere: Journal of Climate, v. 12, p. 3156–3163, https://doi.org/10.1175/1520-0442(1999)012<3156:AGPVAD>2.0.CO;2

Freeman, K. H., and Colarusso, L. A., 2001, Molecular and isotopic records of C_4 grassland expansion in the late Miocene: Geochimica et Cosmochimica Acta, v. 65, n. 9, p. 1439–1454, https://doi.org/10.1016/S0016-7037(00)00573-1

Gaillardet, J., Dupré, B., Louvat, P., and Allegre, C., 1999, Global silicate weathering and CO_2 consumption rates deduced from the chemistry of large rivers: Chemical Geology, v. 159, n. 1–4, p. 3–30, https://doi.org/10.1016/S0009-2541(99)00031-5

Gerrits, A. M. J., Savenije, H. H. G., Veling, E. J. M., and Pfister, L., 2009, Analytical derivation of the Budkyko curve based on rainfall characteristics and a simple evaporation model: Water Resources Research, v. 45, n. 4, https://doi.org/10.1029/2008WR007308

Gibbs, M. T., Bluth, G. J. S., Fawcett, P. J., and Kump, L. R., 1999, Global chemical erosion over the last 250

MY: Variations due to changes in paleogeography, paleoclimate, and paleogeology: American Journal of Science, v. 299, n. 7–9, p. 611–651, https://doi.org/10.2475/ajs.299.7-9.611

Goddéris, Y., François, L. M., Probst, A., Schott, J., Moncoulon, D., Labat, D., and Viville, 2006, Modeling weathering processes at the catchment scale: The WITCH numerical model: Geochimica et Cosmochimica Acta, v. 70, n. 5, p. 1128–1147, https://doi.org/10.1016/j.gca.2005.11.018

Green, J. K., Konings, A. G., Alemohammad, S. H., Berry, J., Entekhabi, D., Kolassa, J., Lee, J.-E., and Gentine, P., 2017, Regionally strong feedbacks between the atmosphere and terrestrial biosphere: Nature Geoscience, v. 10, n. 6, p. 410–414, https://doi.org/10.1038/ngeo2957

Greve, P., Gudmundsson, L., Orlowsky, B., and Seneviratne, S. I., 2015, Introducing a probabilistic Budyko framework: Geophysical Research Letters, v. 42, n. 7, p. 2261–2269, https://doi.org/10.1002/2015GL063449

Grothendieck, G., 2013, nls2: non-linear regression with brute force: R package, v. 0.2.

Hendricks, M. B., DePaolo, D. J., and Cohen, R. C., 2000, Space and time variation of $\delta^{18}O$ and δD in precipitation: Can paleotemperature be estimated from ice cores?: Global Biogeochemical Cycles, v. 14, n. 3, p. 851–861, https://doi.org/10.1029/1999GB001198

Hewawasam, T., von Blanckenburg, F., Bouchez, J., Dixon, J. L., Schuessler, J. A., and Maekeler, R., 2013, Slow advance of the weathering front during deep, supply-limited saprolite formation in the tropical Highlands of Sri Lanka: Geochimica et Cosmochimica Acta, v. 118, p. 202–230, https://doi.org/10.1016/j.gca.2013.05.006

Ibarra, D. E., Caves, J. K., Moon, S., Thomas, D. L., Hartmann, J., Chamberlain, C. P., and Maher, K., 2016, Differential weathering of basaltic and granitic catchments from concentration–discharge relationships: Geochimica et Cosmochimica Acta, v. 190, p. 265–293, https://doi.org/10.1016/j.gca.2016.07.006

Ibarra, D. E., Moon, S., Caves, J. K., Chamberlain, C. P., and Maher, K., 2017, Concentration–discharge patterns of weathering products from global rivers: Acta Geochimica, v. 36, n. 3, p. 405–409, https://doi.org/10.1007/s11631-017-0177-z

Jaramillo, C. A., Rueda, M. J., and Mora, G., 2006, Cenozoic plant diversity in the neotropics: Science, v. 311, n. 5769, p. 1893–1896, https://doi.org/10.1126/science.1121380

Johnson, T. M., and DePaolo, D. J., 1994, Interpretation of isotopic data in groundwater-rock systems: Model development and application to Sr isotope data from Yucca Mountain: Water Resources Research, v. 30, n. 5, p. 1571–1587, https://doi.org/10.1029/94WR00157

Kelly, E. F., Chadwick, O. A., and Hilinski, T. E., 1998, The effect of plants on mineral weathering, in Plant-induced soil changes: Processes and feedbacks: Dordrecht, Springer, Developments in Biogeochemistry, v. 4, p. 21–53, https://doi.org/10.1007/978-94-017-2691-7_2

Kleidon, A., and Heimann, M., 2000, Assessing the role of deep rooted vegetation in the climate system with model simulations: Mechanism, comparison to observations and implications for Amazonian deforestation: Climate Dynamics, v. 16, n. 2–3, p. 183–199, https://doi.org/10.1007/s003820050012

Kleidon, A., Fraedrich, K., and Heimann, M., 2000, A green planet versus a desert world: Estimating the effect of vegetation on the land surface of climate: Climate Change, v. 44, n. 4, p. 471–493, https://doi.org/10.1023/A:1005559518889

Knoll, A. H., 2003, The geological consequences of evolution: Geobiology, v. 1, n. 1, p. 3–14, https://doi.org/10.1046/j.1472-4669.2003.00002.x

Knoll, M. A., and James, W. C., 1987, Effect of the advent and diversification of vascular land plants on mineral weathering through geologic time: Geology, v. 15, n. 12, p. 1099–1102, https://doi.org/10.1130/0091-7613(1987)15<1099:EOTAAD>2.0.CO;2

Koster, R. D., Fekete, B. M., Huffman, G. J., and Stackhouse, P. W., 2006, Revisiting a hydrological analysis framework with International Satellite Land Surface Climatology Project Initiative 2 rainfall, net radiation, and runoff fields: Journal of Geophysical Research-Atmospheres, v. 111, n. D22, https://doi.org/10.1029/2006JD007182

Kump, L. R., and Arthur, M. A., 1997, Global Chemical Erosion during the Cenozoic: Weatherability Balances the Budgets, in Ruddiman, W. F., editor, Tectonic Uplift and Climate Change: Boston, Massachusetts, Springer US, p. 399–426, https://doi.org/10.1007/978-1-4615-5935-1_18

Kump, L. R., Brantley, S. L., and Arthur, M. A., 2000, Chemical weathering, atmospheric CO_2, and climate: Annual Review of Earth and Planetary Sciences, v. 28, p. 611–667, https://doi.org/10.1146/annurev.earth.28.1.611

Labat, D., Goddéris, Y., Probst, J.-L., and Guyot, J.-L., 2004, Evidence for global runoff increase related to climate warming: Advances in Water Resources, v. 27, n. 6, p. 631–642, https://doi.org/10.1016/j.advwatres.2004.02.020

Läderach, A., and Sodemann, H., 2016, A revised picture of the atmospheric moisture residence time: Geophysical Research Letters, v. 43, n. 2, p. 924–933, https://doi.org/10.1002/2015GL067449

Landeweert, R., Hoffland, E., Finlay, R. D., Kuyper, T. W., and van Breemen, N., 2001, Linking plants to rocks: Ectomycorrhizal fungi mobilize nutrients from minerals: Trends in Ecology & Evolution, v. 16, n. 5, p. 248–254, https://doi.org/10.1016/S0169-5347(01)02122-X

Le Hir, G., Donnadieu, Y., Goddéris, Y., Meyer-Berthaud, B., Ramstein, G., and Blakey, R. C., 2011, The climate change caused by the land plant invasion in the Devonian: Earth and Planetary Science Letters, v. 310, n. 3–4, p. 203–212, https://doi.org/10.1016/j.epsl.2011.08.042

Lee, C.-T., Caves, J., Jiang, H., Cao, W., Lenardic, A., McKenzie, N. R., Shorttle, O., Yin, Q.-Z., and Dyer, J., 2018, Deep mantle roots and continental emergence: Implications for whole-Earth elemental cycling, long-term climate, and the Cambrian explosion: International Geology Review, v. 60, n. 4, p. 431–448, https://doi.org/10.1080/00206814.2017.1340853

Lee, J.-E., and Boyce, C. K., 2010, Impact of the hydraulic capacity of plants on water and carbon fluxes in tropical South America: Journal of Geophysical Research-Atmospheres, v. 115, n. D3, https://doi.org/10.1029/2010JD014568

Lee, J.-E., Lintner, B. R., Neelin, J. D., Jiang, X., Gentine, P., Boyce, C. K., Fisher, J. B., Perron, J. T., Kubar, T. L., Lee, J., and Worden, J., 2012, Reduction of tropical land region precipitation variability via transpiration: Geophysical Research Letters, v. 39, n. 19, https://doi.org/10.1029/2012GL053417

Li, D. D., Jacobson, A. D., and McInerney, D. J., 2014, A reactive-transport model for examining tectonic and climatic controls on chemical weathering and atmospheric CO_2 consumption in granitic regolith: Chemical Geology, v. 365, p. 30–42, https://doi.org/10.1016/j.chemgeo.2013.11.028

Li, G., and Elderfield, H., 2013, Evolution of carbon cycle over the past 100 million years: Geochimica et Cosmochimica Acta, v. 103, p. 11–25, https://doi.org/10.1016/j.gca.2012.10.014

Lucas, Y., 2001, The Role of Plants in Controlling Rates and Products of Weathering: Importance of Biological Pumping: Annual Review of Earth and Planetary Sciences, v. 29, n. 1, p. 135–163, https://doi.org/10.1146/annurev.earth.29.1.135

Jongmans, A. G., van Breemen, N., Lundström, U., van Hees, P. A. W., Finlay, R. D., Srinivasan, M., Unestam, T., Giesler, R., Melkerud, P. A., and Olsson, M., 1997, Rock-eating fungi: Nature, v. 389, n. 6652, p. 682–683, https://doi.org/10.1038/39493

Maher K., 2010, The dependence of chemical weathering rates on fluid residence time: Earth and Planetary Science Letters, v. 294, n. 1–2, p. 101–110, https://doi.org/10.1016/j.epsl.2010.03.010

—— 2011, The role of fluid residence time and topographic scales in determining chemical fluxes from landscapes: Earth and Planetary Science Letters, v. 312, n. 1–2, p. 48–58, https://doi.org/10.1016/j.epsl.2011.09.040

Maher, K., and Chamberlain, C. P., 2014, Hydrologic regulation of chemical weathering and the geologic carbon cycle: Science, v. 343, n. 6148, p. 1502–1504, https://doi.org/10.1126/science.1250770

Maher K., Steefel C. I., White, A. F., and Stonestrom, D. A., 2009, The role of reaction affinity and secondary minerals in regulating chemical weathering rates at the Santa Cruz soil chronosequences, California: Geochimica et Cosmochimica Acta, v. 73, n. 10, p. 2804–2831, https://doi.org/10.1016/j.gca.2009.01.030

McCormack, M. L., Adams, T. S., Smithwick, E. A. H., and Eissenstat, D. M., 2012, Predicting fine root lifespan from plant functional traits in temperate trees: New Phytologist, v. 195, n. 4, p. 823-831, https://doi.org/10.1111/j.1469-8137.2012.04198.x

McElwain, J. C., and Punyasena, S. W., 2007, Mass extinction events and the plant fossil record: Trends in Ecology and Evolution, v. 22, n. 10, p. 548–557, https://doi.org/10.1016/j.tree.2007.09.003

McKenzie, N. R., Horton, B. K., Loomis, S. E., Stockli, D. F., Planavsky, N. J., and Lee, C.-T. A., 2016, Continental arc volcanism as the principal driver of icehouse-greenhouse variability: Science, v. 352, n. 6284, p. 444–447, https://doi.org/10.1126/science.aad5787

Mills, B., Lenton, T. M., and Watson, A. J., 2014, Proterozoic oxygen rise linked to shifting balance between seafloor and terrestrial weathering: Proceedings of the National Academy of Sciences of the United States of America, v. 111, n. 25, p. 9073–9078, https://doi.org/10.1073/pnas.1321679111

Misra, S., and Froelich, P. N., 2012, Lithium isotope history of Cenozoic seawater: Changes in silicate weathering and reverse weathering: Science, v. 335, n. 6070, p. 818–823, https://doi.org/10.1126/science.1214697

Mix, H. T., Winnick, M. J., Mulch, A., and Chamberlain, C. P., 2013, Grassland expansion as an instrument of hydrologic change in Neogene western North America: Earth and Planetary Science Letters, v. 377–378, p. 73–83, https://doi.org/10.1016/j.epsl.2013.07.032

Montañez, I. P., 2013, Modern soil system constraints on reconstructing deep time atmospheric CO_2: Geochimica et Cosmochimica Acta, v. 101, p. 57–75, https://doi.org/10.1016/j.gca.2012.10.012

Mooney, H. A., Drake, B. G., Luxmoore, R. J., Oechel, W. C., and Pitelka, L. F., 1991, Predicting Ecosystem Responses to Elevated CO_2 Concentrations: What has been learned from laboratory experiments on plant physiology and field observations: BioScience, v. 41, n. 2, p. 96–104, https://doi.org/10.2307/1311562

Mora, C. I., Driese, S. G., and Colarusso, L. A., 1996, Middle and Late Paleozoic atmospheric CO_2 levels from soil carbonate and organic matter: Science, v. 271, n. 5252, p. 1105–1107, https://doi.org/10.1126/science.271.5252.1105

Moulton, K. L., and Berner, R. A., 1998, Quantification of the effect of plants on weathering: Studies in Iceland: Geology, v. 26, n. 10, p. 895–898, https://doi.org/10.1130/0091-7613(1998)026<0895:QOTEOP>2.3.CO;2

Moulton, K. L., West, J., and Berner, R. A., 2000, Solute flux and mineral mass balance approaches to the quantification of plant effects on silicate weathering: American Journal of Science, v. 300, n. 7, p. 539–570, https://doi.org/10.2475/ajs.300.7.539

Mueller, K. E., Hobbie, S. E., Oleksyn, J., Reich, P. B., and Eissenstat, D. M., 2012, Do evergreen and deciduous trees have different effects on net N mineralization in soils?: Ecology, v. 93, n. 6, p. 1463–1472, https://doi.org/10.1890/11-1906.1

Oerter, E. J., and Amundson, R., 2016, Climate controls on spatial and temporal variations in the formation of pedogenic carbonate in the western Great Basin of North America: Geological Society of America Bulletin, v. 128, n. 7–8, p. 1095–1104, https://doi.org/10.1130/B31367.1

Óskarsson, B. V., Riishuus, M. S., and Arnalds, O., 2012, Climate-dependent chemical weathering of volcanic soils in Iceland: Geoderma, v. 189–190, p. 635–651, https://doi.org/10.1016/j.geoderma.2012.05.030

Pagani, M., Caldeira, K., Berner, R., and Beerling, D. J., 2009, The role of terrestrial plants in limiting atmospheric CO_2 decline over the past 24 million years: Nature, v. 460, p. 85–88, https://doi.org/10.1038/nature08133

Pfefferkorn, H. W., and Wang, J., 2009, *Stigmariopsis, Stigmaria asiatica*, and the survival of the *Sigillaria brardii-ichthyolepis* group in the tropics of the late Pennsylvanian and Early Permian: Palaeoworld, v. 18, n. 2–3, p. 130–135, https://doi.org/10.1016/j.palwor.2009.04.005

Quirk, J., Beerling, D. J., Banwart, S. A., Kakonyi, G., Romero-Gonzalez, M. E., and Leake, J. R., 2012,

Evolution of trees and mycorrhizal fungi intensifies silicate mineral weathering: Biology Letters, v. 8, n. 6, p. 1006–1011, https://doi.org/10.1098/rsbl.2012.0503

Quirk, J., Leake, J. R., Banwart, S. A., Taylor, L. L., and Beerling, D. J., 2014, Weathering by tree-root-associating fungi diminishes under simulated Cenozoic atmospheric CO_2 decline: Biogeosciences, v. 11, p. 321–331, https://doi.org/10.5194/bg-11-321-2014

Roderick, M. L., Sun, F., Lim, W. H., and Farquhar, G. D., 2014, A general framework for understanding the response of the water cycle to global warming over land and ocean: Hydrology and Earth System Sciences, v. 18, n. 5, p. 1575–1589, https://doi.org/10.5194/hess-18-1575-2014

Ronov, A. B., Khain, V. E., Balukhovsky, A. N., and Seslavinsky, K. B., 1980, Quantitative analysis of Phanerozoic sedimentation: Sedimentary Geology, v. 25, n. 4, p. 311–325, https://doi.org/10.1016/0037-0738(80)90067-6

Royer, D. L., Donnadieu, Y., Park, J., Kowalczyk, J., and Gooderis, Y., 2014, Error analysis of CO_2 and O_2 estimates from the long-term geochemical model GEOCARBSULF: American Journal of Science, v. 314, n. 9, p. 1259–1283, https://doi.org/10.2475/09.2014.01

Salati, E., Dall'Olio, A., Matsui, E., and Gat, J. R., 1979, Recycling water in the Amazon Basin: An isotopic study: Water Resources Research, v. 15, n. 5, p. 1250–1258, https://doi.org/10.1029/WR015i005p01250

Schwartzman, D. W., and Volk, T., 1989, Biotic enhancement of weathering and the habitability of Earth: Nature, v. 340, p. 457–459, https://doi.org/10.1038/340457a0

Sellers, P. J., Bounoua, L., Collatz, G. J., Randall, D. A., Dazlich, D. A., Los, S. O., Berry, J. A., Fung, I., Tucker, C. J., Field, C. B., and Jensen, T. G., 1996, Comparison of Radiative and Physiological Effects of Doubled Atmospheric CO_2 on Climate: Science, v. 271, n. 5254, p. 1402–1406, https://doi.org/10.1126/science.271.5254.1402

Sheldon, N. D., Chakrabarti, R., Retallack, G. J., and Smith, R. M. H., 2014, Contrasting geochemical signatures on land from the Middle and Late Permian extinction events: Sedimentology, v. 61, n. 6, p. 1812–1829, https://doi.org/10.1111/sed.12117

Shukla, J., and Mintz, Y., 1982, Influence of Land-Surface Evapotranspiration on the Earth's Climate: Science, v. 215, n. 4539, p. 1498–1501, https://doi.org/10.1126/science.215.4539.1498

Soetaert, K., 2016, rootSolve: Nonlinear root Finding, Equilibrium and Steady-State Analysis of Ordinary Differential Equations: R package, v. 1.7.

Stone, E. L., and Kalisz, P. J., 1991, On the maximum extent of tree roots: Forest Ecology and Management, v. 46, n. 1–2, p. 59–102, https://doi.org/10.1016/0378-1127(91)90245-Q

Strömberg, C. A. E., 2011, Evolution of grasses and grassland ecosystems: Annual Review of Earth and Planetary Sciences, v. 39, p. 517–544, https://doi.org/10.1146/annurev-earth-040809-152402

Swann, A. L. S., Hoffman, F. M., Koven, C. D., and Randerson, J. T., 2016, Plant responses to increasing CO_2 reduce estimates of climate impacts on drought severity: Proceedings of National Academy of Sciences of the United States of America, v. 113, p. 10019–10024, https://doi.org/10.1073/pnas.1604581113

Taylor, L. L., Leake, J. R., Quirk, J., Hardy, K., Banwart, S. A., and Beerling, D. J., 2009, Biological weathering and the long-term carbon cycle: Integrating mycorrhizal evolution and function into the current paradigm: Geobiology, v. 7, n. 2, p. 171–191, https://doi.org/10.1111/j.1472-4669.2009.00194.x

Taylor, L., Banwart, S., Leake, J., and Beerling, D. J., 2011, Modeling the evolutionary rise of ectomycorrhiza on sub-surface weathering environments and the geochemical carbon cycle: American Journal of Science, v. 311, n. 5, p. 369–403, https://doi.org/10.2475/05.2011.01

Taylor, L. L., Banwart, S. A., Valdes, P. J., Leake, J. R., and Beerling, D. J., 2012, Evaluating the effects of terrestrial ecosystems, climate and carbon dioxide on weathering over geological time: A global-scale process-based approach: Philosophical Transactions of the Royal Society of London, Series B, Biological Sciences, v. 367, n. 1588, p. 565–582, https://doi.org/10.1098/rstb.2011.0251

Thomas, D. L., Bird, D. K., Arnórsson, S., and Maher, K., 2016, Geochemistry of CO_2-rich waters in Iceland: Chemical Geology, v. 444, p. 158–179, https://doi.org/10.1016/j.chemgeo.2016.09.002

Thorley, R. M. S., Taylor, L. L., Banwart, S. A., Leake, J. R., and Beerling, D. J., 2015, The role of forest trees and their mycorrhizal fungi in carbonate rock weathering and its significance for global carbon cycling: Plant, Cell & Environment, v. 38, n. 9, p. 1947–1961, https://doi.org/10.1111/pce.12444

Trabucco, A., and Zomer, R. J., 2009, Global aridity index (global-aridity) and global potential evapo-transpiration (global-PET) geospatial database: CGIAR Consortium for Spatial Information.

Uchikawa, J., and Zeebe, R. E., 2008, Influence of terrestrial weathering on ocean acidification and the next glacial inception: Geophysical Research Letters, v. 35, n. 23, https://doi.org/10.1029/2008GL035963

Urey, H. C., 1952, The planets: Their origin and development: New Haven, Connecticut, Yale University Press, 245 p.

van der Ent, R. J., Savenije, H. H. G., Schaefli, B., and Steele-Dunne, S. C., 2010, Origin and fate of atmospheric moisture over continents: Water Resources Research, v. 46, n. 9, p. W09525, https://doi.org/10.1029/2010WR009127

Volk, T., 1987, Feedbacks between weathering and atmospheric CO_2 over the last 100 million years: American Journal of Science, v. 287, n. 8, p. 763–779, https://doi.org/10.2475/ajs.287.8.763

———— 1989, Rise of angiosperms as a factor in long-term cooling: Geology, v. 17, n. 2, p. 107–110, https://doi.org/10.1130/0091-7613(1989)017<0107:ROAAAF>2.3.CO;2

von Blanckenburg, F., Bouchez, J., Ibarra, D. E., and Maher, K., 2015, Stable runoff and weathering fluxes into the oceans over Quaternary climate cycles: Nature Geoscience, v. 8, n. 7, p. 538–542, https://doi.org/10.1038/ngeo2452

Walker, J. C., Hays, P. B., and Kasting, J. F., 1981, A negative feedback mechanism for the long-term stabilization of Earth's surface temperature: Journal of Geophysical Research-Oceans, v. 86, n. C10, p. 9776–9782, https://doi.org/10.1029/JC086iC10p09776

West, A. J., Galy, A., and Bickle, M., 2005, Tectonic and climatic controls on silicate weathering: Earth and Planetary Science Letters, v. 235, n. 1–2, p. 211–228, https://doi.org/10.1016/j.epsl.2005.03.020

White, A. F., and Blum, A. E., 1995, Effects of climate on chemical weathering in watersheds: Geochimica et Cosmochimica Acta, v. 59, n. 9, p. 1729–1747, https://doi.org/10.1016/0016-7037(95)00078-E

Winnick, M. J., and Maher, K., 2018, Relationships between CO_2, thermodynamic limits on silicate weathering, and the strength of the silicate weathering feedback: Earth and Planetary Science Letters, v. 485, p. 111–120, https://doi.org/10.1016/j.epsl.2018.01.005

Winnick, M. J., Chamberlain, C. P., Caves, J. K., and Welker, J. M., 2014, Quantifying the isotopic "continental effect": Earth and Planetary Science Letters, v. 406, p. 123–133, https://doi.org/10.1016/j.epsl.2014.09.005

Wymore, A. S., Brereton, R. L., Ibarra, D. E., Maher, K., and McDowell, W. H., 2017, Critical zone structure controls concentration-discharge relationships and solute generation in forested tropical montane watersheds: Water Resources Research, v. 53, n. 7, p. 6279–6295, https://doi.org/10.1002/2016WR020016

Yapp, C. J., and Poths, H., 1992, Ancient atmospheric CO_2 pressures inferred from natural goethites: Nature, v. 355, p. 342–344, https://doi.org/10.1038/355342a0

–––– 1994, Productivity of pre-vascular continental biota inferred from the $Fe(CO_3)OH$ content of goethite: Nature, v. 368, p. 49–51, https://doi.org/10.1038/368049a0

Zeebe, R. E., 2012, LOSCAR: Long-term Ocean-atmosphere-Sediment CArbon cycle Reservoir Model v2.0.4: Geoscientific Model Development, v. 5, n. 1, p. 149–166, https://doi.org/10.5194/gmd-5-149-2012

Zeebe, R. E., and Caldeira, K., 2008, Close mass balance of long-term carbon fluxes from ice-core CO_2 and ocean chemistry records: Nature Geoscience, v. 1, n. 5, p. 312–315, https://doi.org/10.1038/ngeo185

Zhang, L., Glen, W. R., and Walker, G. R., 1999, Predicting the effect of vegetation changes on catchment average water balance: Cooperative Research Center for Catchment Hydrology, Technical Report 99/12, 12 p.

Zhang, L., Hickel, K., Dawes, W. R., Chiew, F. H. S., Western, A. W., and Briggs, P. R., 2004, A rational function approach for estimating mean annual evapotranspiration: Water Resources Research, v. 40, n. 2, https://doi.org/10.1029/2003WR002710

Zhu, Z., Piao, S., Myneni, R. B., Huang, M., Zeng, Z., Canadell, J. G., Ciais, P., Sitch, S., Friedlingstein, P., Arneth, A., Cao, C., Cheng, L., Kato, E., Koven, C., Li, Y., Xu, L., Liu, Y., Liu, R., Mao, J., Pan, Y., Peng, S., Peñuelas, Poulter, B., Pugh, T. A. M., Stocker, B. D., Viovy, N., Wang, X., Wang, Y., Xiao, Z., Hui, Y., Zaehle, S., and Zeng, N., 2016, Greening of the Earth and its drivers: Nature Climate Change, v. 6, n. 8, p. 791–795, https://doi.org/10.1038/nclimate3004